1

Cancrinite-group minerals. Crystal-chemical description and

properties under non-ambient conditions: A review

G. Diego Gatta and Paolo Lotti

Running title: H*P*-H*T* crystal chemistry of cancrinite-group minerals

Abstract, Keywords

Introduction

Crystal chemistry of cancrinite-group minerals

     - The "cancrinite subgroup"

     - *The "davyne subgroup"*

     - Natural occurrence of cancrinite-group minerals

Description of the compressional and expansion behavior: the equations of state

Compressional behavior of the cancrinite-group minerals

Thermal behavior of cancrinite-group minerals

Mechanisms of crystal structure deformation at non-ambient conditions

     - Mechanisms of framework deformation

     - Behavior of extraframework population at non-ambient conditions

Implications

Acknowledgements, References

Tables and Figures

Corresponding author: G. Diego GATTA

Dipartimento di Scienze della Terra
Università degli Studi di Milano
Via Botticelli, 23
I-20133 Milano, Italy
Tel. +39 02 503 15607, Fax +39 02 503 15597
E-Mail: diego.gatta@unimi.it

31   **Cancrinite-group minerals. Crystal-chemical description and**

32   **properties under non-ambient conditions: A review**

33   [1,2]**G. Diego Gatta** and [1]**Paolo Lotti**

34   [1]Dipartimento di Scienze della Terra, Università degli Studi di Milano, Via Botticelli 23,

35   I-20133 Milano, Italy

36   [2]CNR - Istituto di Cristallografia, Sede di Bari, Via G. Amendola 122/o,

37   I-70126 Bari, Italy

38

39   **Abstract**

40   This is a review of the thermal and compressional behavior of cancrinite-group minerals

41   with a description of the mechanisms, at the atomic scale, that govern their (P,T)-induced structure

42   evolution. The open-framework structure of this group of feldspathoids is characterized by the

43   [CAN] topology, which contains large parallel channels (confined by 12-membered rings of

44   tetrahedra), surrounded by columns of cages. At least two structural "subgroups" can be identified

45   according to the nature of the constituents filling the cages, irrespective of the channel population.

46   The minerals of the "cancrinite subgroup" show [NaH$_2$O]$^+$ clusters into the cages and those of the

47   "davyne subgroup" contains [CaCl]$^+$ clusters. Beside a similar bulk compressibility and expansivity

48   at room conditions for all the minerals of the group, a different elastic anisotropy, coupled with

49   different deformation mechanisms of the tetrahedral framework, were found to be mainly controlled

50   by the nature of the population filling the cages. The role played by the channel populations appear

51   being secondary. These experimental findings allow us to provide a model of the structure evolution

52   in response to the different cage content, *i.e.* NaH$_2$O$^+$ and CaCl$^+$.

53   The high-temperature studies of the hydrous members of the cancrinite subgroup reveal a

54   slow dehydration process, often irreversible at the time-scale of the experiments and leading to

55   quasi-anhydrous high-temperature forms which keep their crystallinity even up to 800-900 K (at

56   room P). The experiments at high pressure on the cancrinite-group minerals show a high-P stability,

57   at least up to 7-8 GPa (at room-T), which is quite surprising if we consider their microporous

58   nature. The P-induced stability is the effect of a pronounced structural flexibility, which in turn is

59   based mainly on tilting of rigid tetrahedra around O atoms that behave as hinges. The character and

60   the mechanisms that govern the (P,T)-induced $P6_3$-to-$P6_3/m$ phase transition in the compounds of

61   davyne subgroup are also discussed.

62

Introduction

Feldspathoids are a loosely-defined class of minerals with a structure characterized by a three-dimensional framework of linked SiO_4 and AlO_4 (more rarely PO_4 or BeO_4) tetrahedra. This framework contains open cavities (in the form of channels and cages), usually occupied by cations (mainly Na^+, K^+, Ca^{2+}), anions (mainly CO_3^{2-}, SO_4^{2-}, Cl^-) and molecules (mainly H_2O). Compared with feldspars, the aluminosilicate feldspathoids are deficient in SiO_2. They occur in a wide variety of geological environments and conditions, from sedimentary to alkali-rich SiO_2-poor igneous rocks or metamorphic and metasomatic rocks, from crustal to upper mantle conditions. Some feldspathoids have been found in meteorites (*e.g.* in carbonaceous chondrites, Grossman 1980).

This class of minerals is the major host of C, S or Cl structurally incorporated in silicates. The structural diversity of feldspathoids is reflected by their complex systematics with at least three different principal families: analcime-leucite (*e.g.* Gatta et al. 2006, 2008a), nepheline-kalsilite (*e.g.* Gatta and Angel 2007; Gatta et al. 2010, 2011) and cancrinite-sodalite (*e.g.* Gatta et al. 2012a; Lotti et al. 2012; Löns and Schulz 1967). Minerals of the melilite family (*i.e.* melilite *sensu stricto*, gehlenite and akermanite) are also considered as feldspathoids (Edgar 1984). A comprehensive overview on the structures of feldspathoids is reported in Merlino (1984).

When compared to other silicates, only a modest number of experiments have been devoted to cancrinite-group minerals at high pressure or high temperature. Some *in situ* experiments at high temperature on the most important member of the group (*i.e.* cancrinite *sensu stricto*) actually provided conflicting results (Hassan 1996a, 1996b; Sirbescu and Jenkins 1999; Hassan et al. 2006; Isupova et al. 2010; Gatta et al. 2014). A full characterization of the phase stability fields of cancrinite-group minerals and of the reactions at the field boundaries is still missing or limited to restricted experimental conditions (*e.g.* Sirbescu and Jenkins 1999 and references therein). To overcome this deficiency, we have recently conducted a series of *in situ* experiments on the behavior of cancrinite-group minerals at non-ambient conditions (*i.e.* high pressure, low and high

4

90   temperature), as part of a wider research project on microporous materials at extreme conditions

91   (*e.g.* Gatta et al. 2012a, 2013a, 2013b; 2014; Lotti et al. 2012, 2014a, 2014b; Lotti 2014).

92   The aim of this manuscript is a synthesis of previously published data on the behavior of

93   cancrinite-group minerals at non-ambient conditions, in order to provide a model of their thermo-

94   elastic behavior and of the main deformation mechanisms, at the atomic scale, in response to the

95   applied temperature (T) and pressure (P).   In particular, the role played by the different

96   extraframework constituents is reviewed and discussed.

97

98   **Crystal chemistry of cancrinite-group minerals**

99   Minerals of the cancrinite group share the tetrahedral [CAN] framework-type, built by the

100   stacking of layers made by unconnected single six-membered rings of tetrahedra (hereafter S6R's)

101   occupying A or B positions, respectively, according to an ···AB(A)··· sequence (Gies et al. 1999;

102   Baerlocher et al. 2007). Each S6R is connected to three rings in adjacent layers, giving rise to the

103   three-dimensional   framework   (Figure   1,   see   also   http://www.iza-

104   structure.org/databases/Catalog/ABC_6.pdf). The [CAN] framework contains columns of base-

105   sharing cages (*i.e. can* units or cancrinite cages), where the bases correspond to the single six-

106   membered rings perpendicular to the **c**-axis (S6R⊥[0001], Figure 1). These columns surround

107   parallel channels to [0001] and are confined by twelve-membered rings of tetrahedra (12R) (Figure

108   1). The framework can also be described as made of double *zigzag* chains of tetrahedra (*dzc* units,

109   Smith 2000), made by edge-sharing four-membered rings (S4R), running along the **c**-axis, which

110   border 6R-windows∠[0001] linking cages and channels (Figure 1). The topological symmetry of

111   the [CAN] framework is $P6_3/mmc$ (Baerlocher et al. 2007). Overall, materials with [CAN]

112   framework type are considered as "microporous materials" (*sensu* Rouquerol et al. 1994), having

113   cavities with free diameters shorter than 2 nm.

114   Twelve mineralogical species sharing the [CAN] topology have so far been reported

115   (Bonaccorsi and Merlino 2005; Pekov et al. 2011a) (Table 1) and eleven of them show an

116   aluminosilicate framework; the only exception is tiptopite, with a P/Be-framework (Table 1; Peacor

117   et al. 1987). In cancrinite-group minerals, the Si/Al-distribution of the $(Al_6Si_6O_{24})^{6-}$-framework is

118   fully ordered, with a lowering of the symmetry from $P6_3/mmc$ to $P6_3$ (or $P6_3/m$), with only rare

119   exceptions (Rastsvetaeva et al. 2007; Ogorodova et al. 2009). In this group of minerals, the

120   extraframework population can be subdivided according to the structural voids, namely: 1) the *can*

121   cages and 2) the 12R-channels. Only two mutually exclusive configurations of the cage constituents

122   are shown by the aluminosilicate cancrinite-group minerals: the first is given by the repetition of

123    $[Na \cdot H_2O]^+$ clusters, so that chains along the columns of *can* units arise, and, similarly, the second

124   configuration is represented by chains of $[Ca \cdot Cl]^+$ clusters (Figure 2). In contrast, a complex

125   chemical variability is shown by the 12R-channel population, made by cations, anions and

126   molecular components, though a general scheme can be extrapolated. Na^+ is always the prevailing

127   cation, it can be partially replaced by Ca^{2+} and K^+ in one or two crystallographic sites close to the

128   channel walls (Figure 3); a more complex positional disorder was also reported (*e.g*. Gatta et al.

129   2013a). Nevertheless, a similar bonding environment of cations can be described, with 4-5 bonds to

130   the framework oxygen atoms on the wall-side and a variable coordination with the anionic groups

131   or molecules on the other side. Anions and molecules occupy the center of the channel (Figure 3),

132   often in mutually-exclusive split positions, so that several possible configurations can occur within

133   the same channel. These configurations can be ordered, leading to superstructures (see next

134   section). The most common anionic and molecular species in cancrinite-group minerals are: CO_3^{2-},

135   SO_4^{2-}, Cl^-, $C_2O_4^{2-}$, PO_4^{3-}, OH^- and H_2O. The most abundant anion is conventionally used as

136   "species-defining criterion" (Bonaccorsi and Merlino 2005; Pekov et al. 2011a).

137   For a comparative and comprehensive analysis of the HP-HT crystal-chemistry of this

138   mineral group, two "subgroups" can be defined: the "cancrinite subgroup", showing chains of

139 [Na·H₂O]⁺ clusters, and the "davyne subgroup", with [Ca·Cl]⁺ chains (Figure 2). In the next

140 sections we describe the crystallochemical features and the occurrences of these isotypic minerals.

141

142   *- The "cancrinite subgroup"*

143   In the structural cages of this subgroup, the Na^+ site is slightly displaced from the

144 S6R⊥[0001]-plane, with a stronger bond to one of the neighboring H_2O-oxygen sites, positioned

145 out of the 3-fold axis approximately at the cage center (Figure 2). Therefore, each H_2O molecule

146 shows a shorter bond to one Na^+ cation and a longer one to the other Na-neighbor, which, in turn, is

147 strongly bonded to the next H_2O molecule (Figure 2). Similarly, Na^+ shows shorter bonds to the

148 three O2 oxygen sites than those to the three O1 sites. As a consequence, a significant deviation

149 from the hexagonal shape is shown by the S6R⊥[0001] (Figure 1). The Na^+ coordination

150 environment can, therefore, be described by a first tetrahedral shell (3·O2 + Ow′) along with a

151 second larger tetrahedral one (3·O1 + Ow″), giving rise to a distorted ditrigonal bipyramid (C.N. =

152 4 + 4).

153   Cancrinite *sensu stricto* $[(Na,Ca)_6(CO_3)_{1.4-1.7}][NaH_2O]_2[Al_6Si_6O_{24}]$ (Table 1; Bonaccorsi and

154 Merlino 2005) is, by far, the most widespread mineral of the group. Its crystal structure was first

155 solved by Pauling (1930), and then refined by Jarchow (1965). Cancrinite contains CO_3^{2-} as main

156 anionic component in the channel voids. The CO_3^{2-} groups occupy the center of the channel in two

157 mutually exclusive and iso-oriented configurations, for which the neighboring cations face an edge

158 of the triangular anionic group, giving rise to two bonds to the closer oxygen atoms (Figure 3). Due

159 to the resulting short C-C contacts, not all the sub-cells can be occupied by the carbonate anions,

160 with positional order/disorder leading also to superstructures (*e.g.* Foit et al. 1973; Grundy and

161 Hassan 1982; Hassan and Buseck 1992).

162   Vishnevite $[(Na,K)_6(SO_4)][NaH_2O]_2[Al_6Si_6O_{24}]$ (Table 1; Hassan and Grundy 1984; Della

163   Ventura et al. 2007) is the (SO_4^{2-})-dominant end-member. Two distinct configurations can be

164   defined for the channel population. The first, with $[Na_3(SO_4)]^+$ clusters, is given by the Na^+ cations

165   and sulfate tetrahedral groups at the center of the channel, for which the triangular basis is generally

166   found to point a vertex toward the neighboring Na^+ atoms, so that a single $Na\text{-}O_{SO4}$ bond occurs

167   (Figure 3). The second, with only Na and K sites bonded to the framework oxygens, is commonly

168   associated to vacancies at the anionic sites (at the channel center), in order to avoid too short K-O

169   bonds (Figure 3). A channel can be internally ordered. If there is an ordered distribution of these

170   configurations among adjacent channels, a superstructure with a new unit-cell **a**-parameter, equal to

171    $\sqrt{3}\mathbf{a}_{vish}$, arises. This gives rise to a new mineralogical species called pitiglianoite (Table 1; Merlino

172   et al. 1991; Della Ventura et al. 2005; Bonaccorsi et al. 2007), which shares with vishnevite a

173   common **c**-parameter.

174   Hydroxycancrinite (or "basic cancrinite") is the (OH^-)-dominant end-member of the

175   cancrinite subgroup (Table 1) and is often reported as a synthetic product. In Nature, it is rare and

176   usually represented by intermediate members of the cancrinite-hydroxycancrinite series in the

177   peralkaline plutons of the Kola peninsula, Russia (Pekov et al. 2011a). Kyanoxalite is the $C_2O_4^{2-}$

178   member (Table 1). It is very rare in Nature; minerals of the cancrinite-kyanoxalite series have, up to

179   now, been found only at the Lovozero alkaline pluton, Kola peninsula, Russia (Chukanov et al.

180   2010a; Olysych et al. 2011; Pekov et al. 2011a). Depmeierite is the PO_4^{3-}-dominant member of the

181   cancrinite subgroup (Table 1) and has been reported only from Mt. Karnasurt, Kola peninsula,

182   Russia (Pekov et al. 2011b).

183   Cancrisilite is the only member of the cancrinite group of minerals showing the framework

184   enriched in Si^{4+}, with an ideal $Si^{4+}:Al^{3+}$ ratio of 7:5 (Table 1). This leads to a disordered Si/Al-

185   distribution in the tetrahedral framework, with an increase in symmetry from $P6_3$ to $P6_3mc$

186   (Ogorodova et al. 2009).

187

188   *- The "davyne subgroup"*

189   The davyne-subgroup minerals contain chains of alternating $[Ca \cdot Cl]^+$ clusters. The Ca^{2+} site

190   lies close to the $S6R \perp [0001]$ "plane" (*i.e.* the cage basis) and is bonded to the three O2 and the

191   three O1 atoms, showing similar bond lengths (Figure 2). Therefore, only a small deviation from the

192   perfect hexagonal shape of the $S6R \perp [0001]$ is observed in davyne-subgroup minerals (Figure 1).

193   The Cl^- anion is placed approximately at the center of the cage in three mutually exclusive positions

194   out of the 3-fold axis (Figure 2). Each Ca^{2+} cation is bonded to the two neighboring Cl^-, giving rise

195   to a slightly distorted hexagonal bipyramidal coordination shell (C.N. = 8).

196   Davyne $[(Na,K)_6(SO_4,Cl)][CaCl]_2[Al_6Si_6O_{24}]$ (Table   1;   Hassan   and   Grundy   1990;

197   Bonaccorsi et al. 1990; Gatta et al. 2013a; Lotti et al. 2014a) and balliranoite $[(Na,Ca)_6(CO_3)_{1.4-}$

198     $_{1.7}][CaCl]_2[Al_6Si_6O_{24}]$ (Table 1; Chukanov et al. 2010b; Gatta et al. 2013b; Lotti et al. 2014b) are

199   the (SO_4^{2-},Cl^-)- and CO_3^{2-}-end-members, respectively, and show a channel configuration analogous

200   to that of vishnevite (for davyne) and cancrinite (for balliranoite) (Figure 3). In microsommite

201   (Table 1; Bonaccorsi et al. 2001), the ordered distribution along the channel of SO_4^{2-} groups and

202   vacancies at the anionic sites (at the channel center) leads to a superstructure similar to that shown

203   by pitiglianoite ($\mathbf{a}_{MIC} = \sqrt{3} \cdot \mathbf{a}_{DAV}$, $\mathbf{c}_{MIC} = \mathbf{c}_{DAV}$), whereas in the pure Cl^--end-member, quadridavyne

204   (Table 1; Bonaccorsi et al. 1994), a different kind of superstructure occurs, with $\mathbf{a}_{QUA} = 2 \cdot \mathbf{a}_{DAV}$ and

205     $\mathbf{c}_{QUA} = \mathbf{c}_{DAV}$.

206

207   *- Natural occurrence of cancrinite-group minerals*

208   Cancrinite-group minerals are typical of silica-undersaturated rocks and rich in alkalis,

209   particularly Na. They are commonly related to alkaline magmatism (Deer et al. 2004). Cancrinite-

210   group minerals are widespread both in intrusive igneous rocks, such as nepheline syenites, and in

211   extrusive rocks, such as phonolites. In addition, they can be found in metasomatic environments

212   related to alkaline magmas and/or limestone wallrocks.

213   Pekov et al. (2011a) suggested the distinction between cancrinite and davyne subgroups to

214   have also a genetic relevance, being the minerals of the first subgroup most commonly found in

215   intrusive environments and those of the second subgroup in effusive and metasomatic settings.

216   Cancrinite-subgroup minerals are widespread in intrusive alkaline magmatic complexes, where they

217   can crystallize: 1) as primary phases during the late-magmatic stage, typical of vein- and dyke-

218   intrusions or pegmatites (*e.g.* Erd and Czamanske 1983; Deer et al. 2004), or 2) as secondary phases

219   from hydrothermal alteration of pre-existing minerals (*e.g.* Bell et al. 1996; Sindern and Kramm

220   2000; Fall et al. 2007).

221   The davyne-subgroup minerals can be typically found in effusive and metasomatic

222   environments, especially in lithic blocks within pyroclastic, tephritic and pumice deposits. They

223   generally occur in cavities of skarn-like rocks, likely formed as thermal metamorphic and

224   metasomatic products, around the magmatic chamber walls (*e.g.* Deer et al. 2004; Fulignati et al.

225   2005; Sapozhnikov 2010; Harlow and Bender 2013).

226

227   **Description of the compressional and expansion behavior: the equations of state**

228   For a comparative analysis of the elastic behavior of cancrinite-group minerals, their volume

229   compressibility and expansivity parameters are here determined by fitting the experimental unit-cell

230   data to *P-V* and *T-V* equations of state. The isothermal Birch-Murnaghan equation of state (BM-

231   EoS) was adopted for the high-pressure data. The BM-EoS is based on the assumption that the

232   strain energy in a solid can be described as a Taylor series in the Eulerian finite strain,

233        $f_e = [(V_0/V)^{2/3} - 1]/2$ (Birch 1947; Angel 2000).

234   In the HP-studies of cancrinite-group minerals (Lotti et al. 2012, 2014a, 2014b; Lotti 2014),

235   the polynomial truncated to third order in energy (III-BM EoS) was used, with the following form:

236        $P = 3K_0f_e(1 + 2f_e)^{5/2}\,[1 + 3/2(K' - 4)f_e]$,

237   where K_0 is the isothermal bulk modulus, $i.e.$ the inverse of the volume compressibility:

238        $K_0 = 1/\beta_V = -V \cdot (\partial P/\partial V)$,

239   and K' is its pressure-derivative ($i.e.$ $K' = \partial K_0/\partial P$). When a BM-EoS is truncated to second order in

240   energy, $K' = 4$ is implied. "Linearized" BM-equations of state, for which the cube of a linear

241   parameter ($e.g.$ unit-cell edge) replaces the volume, were adopted to fit the experimental l-P data

242   and, therefore, to describe the anisotropy of the elastic behavior. The obtained "linear-K_0" (Angel

243   2000) is one third of the inverse of the linear volume compressibility: $K_{l0} = 1/3\beta_l$.

244   The elastic behavior in the low-T range (ca. 110-293 K) was described by Gatta et al.

245   (2012a, 2013a, 2013b) fitting the experimental data with an equation directly derived from the

246   thermodynamic definition of the thermal expansion coefficient:

247        $\alpha_V = V^{-1}(\partial V/\partial T)$, $V(T) = V_0 e^{[\alpha_V(T-T_0)]}$,

248   assuming a constant α_V value due to the low number of the experimental data. The high-temperature

249   elastic behavior of cancrinite was described by Gatta et al. (2014) with a modified second-order

250   polynomial equation proposed by Berman (1988) and implemented in the EOSFIT7 software

251   (Angel et al. 2014):

252        $V(T) = V_0[1 + a_0(T-T_0) - 2(10a_0 + a_1)(T^{1/2} - T_0^{1/2})]$,

253   where $\alpha_V = a_0 + a_1(T - T_0)$, a_0 and a_1 are two refinable parameters.

254

11

Compressional behavior of the cancrinite-group minerals

The *P*-induced evolution of the unit-cell parameters of the studied cancrinite-group minerals is shown in Figure 4, and the elastic parameters, refined from BM-EoS fits, are listed in Table 2. These parameters show that all the studied minerals have similar bulk muduli at room conditions, where the refined K_0 values (~47 GPa) fall in the range so far reported for open-framework silicates (Gatta 2008, 2010; Gatta and Lee 2014). Moreover, all the members of the group share the same elastic anisotropy scheme, where the most compressible direction, along the **c** crystallographic axis, corresponds to the stacking of S6R-layers (Figure 1). Besides the similar anisotropy scheme, the calculated K_a:K_c ratios (Table 2) suggest a different behavior for the cancrinite- and the davyne-subgroup minerals, with elastic anisotropy more pronounced in the formers.

If the *P*-induced elastic response of davyne and balliranoite is virtually identical within estimated standard deviations (Figure 4; Table 2; Lotti et al. 2014a,b), a comparison of the cancrinite and vishnevite behaviors shows a different scenario. Vishnevite clearly shows a significant increase in compressibility, related to a structural re-arrangement of the channel population (Lotti 2014) at *P* > 3.43 GPa. In cancrinite, an apparent softening is observed at higher pressures (*P* > 4.62 GPa; Lotti et al. 2012) by the evolution of the unit-cell parameters with *P*, but without any significant change in the evolution of structural parameters at the atomic scale. For both cancrinite and vishnevite, the change in the elastic behavior at high pressure leads to an increase of the elastic anisotropy (Table 2). Nevertheless, the elastic parameters reported in Table 2 suggest that the minerals of this subgroup share the same bulk compressibility and elastic anisotropy at ambient conditions and, more generally, in the low-*P* regime (Figure 4).

The same conclusion is valid for the synthetic hydroxycancrinite (Table 2), a cancrinite-subgroup compound studied at high-pressure by Oh et al. (2011). It is worth noting that Oh et al. (2011) also reported a subtle discontinuity in the *P-V* data between 1.9 and 2.5 GPa, although not supported by structural data. The only other compound of the cancrinite group studied at high

280   pressure is the synthetic $Na_6Cs_2[Ga_6Ge_6O_{24}]\cdot Ge(OH)_6$ (Gatta and Lee 2008), which is the only one

281   with a non-aluminosilicate framework studied at high pressure. To the different composition of the

282   tetrahedral framework is likely ascribable the reported higher bulk compressibility (Table 2). The

283   pronounced compression in the low-P regime of the $(Ga,Ge)O_4$ tetrahedra is, at least partially,

284   responsible for the lower K_0 and for the elastic stiffening with increasing pressure (as suggested by

285   the higher K'), if compared to the natural compounds all showing a "quasi-rigid" Si- or Al-

286   tetrahedra.

287   All the cancrinite-group compounds studied at high pressure were found to be stable up to

288   the highest pressures investigated (Table 2), with no hints of structural collapse or amorphization. In

289   particular, davyne and balliranoite showed stability up to ~ 7 GPa without phase transitions or

290   change of the compressional behavior (Lotti et al. 2014a, 2014b).

291

292   **Thermal behavior of cancrinite-group minerals**

293   Several studies have been devoted to the high-temperature behavior of cancrinite-group

294   compounds. We will provide a brief overview of the behavior of natural samples, starting from the

295   *in situ* single-crystal X-ray diffraction study of cancrinite *sensu stricto* performed by Gatta et al.

296   (2014), who reported a very slow dehydration process at 748 K, which took 12 days to reach

297   structural relaxation. Similarly, Sirbescu and Jenkins (1999) reported a thermogravimetric analysis

298   of a synthetic sample of cancrinite (0.06 K/min average heating rate) which needed 10 days to fully

299   dehydrate at 1058 K, with an intense weight-loss peak in the range 570-770 K. These results are in

300   good agreement with the structure refinement performed by Gatta et al. (2014) at T above the

301   dehydration temperature (*i.e.* 748 K), showing the presence of residual H_2O molecules within the

302   *can* unit cages. It is worth noting the stability, or metastability, of the "quasi-anhydrous" cancrinite

303   reported by Gatta et al. (2014) at least in the range 748-823 K, above which a broadening of the

304   diffraction peaks suggested an impending decomposition or a severe deterioration of the long-range

13

305   order of the crystal. Interestingly, the dehydration was reported to be irreversible at the time-scale

306   of the experiment, as confirmed by the diffraction data collected after the high-T ramp. The

307   dehydration of a natural cancrinite was also reported by Isupova et al. (2010) by *in situ* single-

308   crystal X-ray diffraction at 623 K, above which a dehydrated form was reported to be crystalline at

309   least up to 823 K. An irreversible dehydration was also reported by Ballirano et al. (1995), on basis

310   of an *ex situ* single-crystal X-ray diffraction experiment at room-T on a cancrinite sample

311   previously heated up to 873 K.

312   These experimental observations may be coupled with the findings of natural partially

313   anhydrous cancrinite crystals in volcanic alkaline rocks at the Eifel region, for which Zubkova et al.

314   (2011) suggested the loss of H_2O in response to the roasting of the crystals during the effusive

315   process. The high-T behavior of a natural cancrinite, showing superstructure reflections along the **c**-

316   axis, was also studied by Hassan et al. (2006) by *in situ* synchrotron X-ray powder diffraction,

317   reporting a discontinuity in the evolution of the unit-cell parameters at 777 K and a complete

318   dehydration at 898 K. Loss of CO_2 was reported to occur at 1223 K by Hassan (1996a) on the basis

319   of a TG-DTG analysis of a natural cancrinite, which was observed to melt at 1528 K. Sirbescu and

320   Jenkins (1999) reported unchanged CO_3^{2-} signals from *ex situ* infra-red analysis of previously

321   heated synthetic cancrinite up to 1153 K, where decomposition to a mixture of nepheline + haüyne

322   was observed.

323   To the best of our knowledge, no high-temperature studies of the SO_4^{2-}-end member of the

324   cancrinite subgroup (*i.e.* vishnevite) are available in the open literature. However, the high-T

325   behavior of the K-rich pitiglianoite was performed by Bonaccorsi et al. (2007) by *in situ* single-

326   crystal X-ray diffraction and FTIR spectroscopy. These authors reported a unit-cell expansion up to

327   499 K, followed by a dehydration process with unit-cell contraction in the range 499-676 K and a

328   further expansion between 676 and 914 K. The dehydration was coupled with a partial and

329   irreversible migration of the channel-K^+ cations into the *can* cages and cage-Na^+ into the channel

14

330   sites, which likely played a role in the minor re-adsorption of H_2O observed with decreasing

331   temperature. These data point out the significant influence of the extraframework constituents on

332   the (P,T)-induced transformations of cancrinite-group minerals. The presence of CO_2 molecules,

333   along with SO_4^{2-} anions, within the structural channels was confirmed by FTIR spectra, which

334   suggested, as reported by Bonaccorsi et al. (2007), a full loss of CO_2 at $T \geq 723$ K.

335   The major difference between the high-T behavior of the cancrinite- and davyne-subgroup

336   minerals can be found in the (nominally) anhydrous nature of the latter. Bonaccorsi et al. (1995)

337   reported the high-T study of both $P6_3$-davyne and $P6_3$-microsommite, by *in situ* single-crystal X-

338   ray diffraction, observing a similar thermal expansion with a clear discontinuity in the evolution of

339   the cell parameters and a decrease of the thermal expansivity along the **c**-axis (Table 2) at 473 (for

340   davyne) and 433 K (for microsommite). This discontinuity is due to the displacive phase transition

341   to the $P6_3/m$ space group, induced by the expansion of the *dzc* chains, *via* tetrahedral tilting, to the

342   geometric limit for which the inter-tetrahedral O3-O4-O3 angle is 180° (O3-O3-O3 in space group

343    $P6_3/m$, Figure 5). This symmetry-constraint prevents a further expansion of the *dzc* chains by

344   tetrahedral tilting and is responsible for the decrease of the thermal expansivity along the [0001]

345   direction.

346   Bonaccorsi et al. (1995) also reported the high-T behavior of a davyne sample with $P6_3/m$

347   symmetry at room conditions, for which insignificant thermal expansion along the **c**-axis was

348   observed even at the low-temperature regime (Table 2). The high-T behavior of microsommite

349   later studied by Bonaccorsi et al. (2001), by *in situ* single-crystal X-ray diffraction and Monte Carlo

350   simulation, in order to define the order-disorder processes of the extraframework population. The

351   authors reported a full disorder (*i.e.* in response to a complete microsommite-to-davyne structure

352   transformation) at the critical temperature of 1023 K.

353   If the T-induced dehydration may act as a destabilizing factor affecting the cancrinite-

354   subgroup compounds, in the nominally anhydrous davyne-subgroup minerals a potential source of

355 thermal instability is represented by the *T*-induced phase transition to the $P6_3/m$ space group, which

356 hinders the deformation mechanisms able to accommodate the structural expansion along the **c**-axis

357 *via* tetrahedral tilting.

358 When not affected by dehydration processes, all minerals of the cancrinite group show

359 comparable bulk thermal expansivities (Hassan et al. 2006; Gatta et al. 2012a, 2013a, 2013b, 2014),

360 and the stacking direction of the 6-rings layers ([0001]-axis) is the most expandable one. Two

361 different anisotropic patterns can be defined for the minerals belonging to the two subgroups, more

362 pronounced for cancrinite-subgroup minerals (Table 2).

363

364 **Mechanisms of crystal structure deformation at non-ambient conditions**

365 *- Mechanisms of framework deformation*

366 The different coordination environment of the Na^+ cation, compared with that of Ca^{2+}

367 (Figure 2), leads to a framework contraction of cancrinite and vishnevite in the (0001) plane already

368 at room conditions. Moreover, beside the different ditrigonal character of the $S6R\perp[0001]$ (Figure

369 1), a different configuration of the channel voids is also observed among the cancrinite-group

370 minerals. In cancrinite subgroup, the $\sim$ 1:1 ratio of the symmetry-independent $O1\text{-}O1_{12R}$ and O3-

371 $O4_{12R}$ diameters (Figure 6) gives an almost circular shape of the section perpendicular to the **c** axis;

372 in davyne subgroup, a markedly hexagonal section occurs (Figure 1), with a smaller effective pore

373 width (*sensu* Baerlocher et al. 2007). In addition, the presence of $[Ca \cdot Cl]^+$ clusters in the cages

374 and/or SO_4^{2-} anions (with associated K^+ cations) in the channels leads to an expansion of the *dzc*

375 chains along [0001] already at room conditions. As a consequence, the *dzc* chains are more

376 expanded in vishnevite than cancrinite and in davyne than balliranoite.

377   The different extraframework population in cancrinite- and davyne-subgroup members is

378 not only the source for the different framework configurations at ambient conditions, but also the

379 cause of the different distortion mechanisms in response to temperature or pressure. In the

380 following paragraphs, we provide a model of the structural evolution of cancrinite-group minerals at

381 non-ambient conditions, on the basis of the high-P studies of Lotti (2014) and Lotti et al. (2012,

382 2014a, 2014b) and the low- and high-T studies of Bonaccorsi et al. (1995, 2007), Hassan et al.

383 (2006), Isupova et al. (2010) and Gatta et al. (2012a, 2013a, 2013b, 2014).

384   The analysis of the T- and P-induced evolution of the Si-O-Al inter-tetrahedral angles shows

385 that two distinct trends can be defined for the cancrinite- and davyne-subgroup minerals,

386 respectively. In cancrinite subgroup, all the four symmetry-independent Si-O-Al angles vary with T

387 or P (Figure 7, Tables 3 and 4 - deposited). In davyne subgroup, no significant variations of the Si-

388 O2-Al angle are observed and the Si-O1-Al angle always shows the greatest change with T or P

389 (Figure 7, Tables 3 and 4). These different trends are the basis for different deformation

390 mechanisms in the two subgroups.

391   The framework deformation along [0001] is controlled by the tilting of the tetrahedra

392 forming the dzc chains, around the O3 and O4 hinges (Figures 1 and 5), which correlates with the

393 Si-O3-Al and Si-O4-Al inter-tetrahedral angles. The behavior of these angles with P and T does not

394 show any significant difference between the two subgroups of minerals (Tables 3 and 4). The same

395 deformation mechanism accommodates the strain along the **c**-axis: the expansion or compression of

396 the dzc chains is well described by the change in the O3-O4-O3 angle (Figures 5 and 6; Tables 3

397 and 4). When the maximum expansion limit of 180° is reached, the displacive phase transition from

398 the $P6_3$ to the $P6_3/m$ space group occurs (Bonaccorsi et al. 1995). Similarly, the reverse transition

399 occurs when pressure is applied to a davyne sample showing $P6_3/m$ symmetry at room conditions

400 (Lotti et al. 2014a).

401   The main differences between the two subgroups are in the mechanisms accommodating the

402   strain within the (0001) plane, mainly governed by the tilting of the tetrahedra around the O1 and

403   O2 hinges, correlated with the Si-O1-Al and Si-O2-Al inter-tetrahedral angles. In cancrinite and

404   vishnevite, a strong variation in the ditrigonal shape of the S6R⊥[0001] occurs in response to T and

405   P, and the bulk compression/expansion is accommodated by both the S4R's (along O3-O4) and by

406   the channels (along O1-O1) (Figure 6; Tables 3 and 4). In contrast, balliranoite and davyne show

407   less intense "ditrigonalization" of the cage bases, and the compression/expansion on the (0001)

408   plane is mainly accommodated by the channel diameters (Figure 6; Tables 3 and 4). Overall, for all

409   the studied minerals, the contribution of the channel voids to the bulk compressibility/expansivity

410   was found to be significantly higher than that of the *can* cages (Lotti 2014).

411

412   *- Behavior of extraframework population at non-ambient conditions*

413   The high-P and low-T studies of cancrinite (Lotti et al. 2012; Gatta et al. 2012a) and

414   vishnevite (Lotti 2014) showed, in response to pressure or low temperature, a compression of the

415   first tetrahedral shell of the Na coordination environment into the cage (involving three O2 and the

416   closer Ow sites) and an anisotropic expansion of the second shell (Tables 3 and 4). In other words,

417   the distortion of the bipyramidal polyhedron is further enhanced in a "compressive" regime (*i.e.*

418   high-P and low-T), leading to an increasingly tetrahedral form of the Na-coordination. In contrast,

419   only minor changes occur for the Ca-O bonds in balliranoite and davyne at the same conditions

420   (Tables 3 and 4; Gatta et al. 2013a, 2013b; Lotti et al. 2014a, 2014b). This markedly different

421   behavior reflects the different evolution with T and P of the Si-O2-Al inter-tetrahedral angle

422   between the two subgroups (Tables 3 and 4). In fact, the inhibited tetrahedral rotation around the O2

423   hinge (Figure 6) in davyne-subgroup minerals prevents the migration of this oxygen toward the

424   Ca^{2+} cation and, as a consequence, a significant compression of the Ca-O2 bonds (Figure 2). Such a

425   different behavior may be ascribed to the nature of the cage cations and their different coordination

18

426   configuration: the longer Ca-O bond lengths, if compared to Na-O ones, can explain the less

427   pronounced compression of the Ca-O2 bonds (than the Na-O2) in response to the applied P (or low-

428   T), leading to different framework deformation mechanisms than those observed in Na-members.

429   The analysis of the high-temperature behavior of cancrinite showed the same mechanisms

430   previously observed at low-T and high-P, but opposite in sign, at least at temperatures below the

431   start of dehydration (Table 4; Hassan et al. 2006; Isupova et al. 2010; Gatta et al. 2014). In response

432   to dehydration, an inversion in the T-induced trend of the Si-O2-Al inter-tetrahedral angle can be

433   observed from the HT studies of Isupova et al. (2010) and Gatta et al. (2014) (Table 4), likely to

434   minimize both the Na-O1 and Na-O2 bond lengths in order to counterbalance the loss of H_2O-

435   oxygen atoms. This mechanism concurs to the stability (or metastability) of the observed quasi-

436   anhydrous form of cancrinite in Nature.

437   The compression/expansion of the chemical bonds of the channel cations (M-$O_{framework}$, $M =$

438   Na, Ca, K) is strictly related to the distortion of the dzc chains along [0001]. In cancrinite,

439   balliranoite and davyne, no substantial change in the coordination of channel cations and anions

440   was observed at non-ambient conditions (Gatta et al. 2012a, 2013a, 2013b; Lotti et al. 2012, 2014a,

441   2014b). Therefore, for these minerals, the channel extraframework population apparently does not

442   have a significant effect on the behavior in response to the applied temperature or pressure. In

443   contrast, a re-arrangement of the channel population apparently occurs in vishnevite at $P \geq 3.43(4)$

444   GPa, coupled with a significant increase in compressibility (Lotti 2014). In vishnevite, a

445   displacement of the SO_4^{2-} tetrahedra around the 6_3-axis is followed by a significant migration of the

446   Na^+ cations towards the center of the channel. However, the marked increase in compressibility and

447   the unusual short K-O bonds suggest a metastable nature of the observed high-P configuration of

448   vishnevite (Lotti 2014). Nevertheless, these data show that even the channel constituents, and in

449   particular the cations bonding environment, might control the behavior and the stability of some

450   cancrinite-group species at non-ambient conditions. This is also substantiated by the high-T

451 behavior of pitiglianoite (Bonaccorsi et al. 2007), for which, at temperatures above the dehydration

452 process, an irreversible Na^+ / K^+ cationic exchange occur between channels and cages, with the

453 larger cations occupying the *can* units in the new high-*T* structural configuration.

454

455 **Implications**

456 The studies performed during the last decade on the behavior of cancrinite-group minerals at

457 non-ambient conditions, and here reviewed, allowed the experimental determination of the thermo-

458 elastic parameters of the most important end-members of this group (Table 2), whose

459 implementation in the thermodynamic datasets can be used for a better modelling of the complex

460 equilibria relating to natural rocks. Often, thermodynamic data (here isothermal compressibility or

461 isobaric thermal expansivity) are "estimated", when not known experimentally (*e.g.* Holland and

462 Powell 2011), giving rise to potentially crude results.

463 The crystal chemistry of cancrinite-group minerals is somehow unique: they are among the

464 few silicates which contain structurally incorporated H_2O and anionic groups as CO_3^{2-}, $C_2O_4^{2-}$,

465 SO_4^{2-} or Cl^-. Their open-frameworks allow also additional molecules to be entrapped into the

466 cavities, including CO_2. Della Ventura et al. (2007, 2008) reported, on the basis of infra-red

467 spectroscopic analyses, the presence of strong rim-to-core inhomogeneities in the volatile

468 composition of cancrinite-group minerals due to a CO_2/CO_3^{2-} substitution, pointing out the

469 sensitiveness of these compounds to the physical-chemical conditions of the crystallization

470 environments and suggesting their potential application as geochemical markers.

471 The high-*T* experiments made on the cancrinite group show that the anhydrous forms keep

472 their crystallinity even at 800-900 K, which is very high temperature for microporous structures.

473 High-*T* studies of cancrinite *sensu stricto* (*e.g.* Sirbescu and Jenkins 1999; Gatta et al. 2014) report

474 slow kinetics of dehydration under equilibrium conditions, if compared to other hydrous

475   microporous silicates, *e.g.* zeolites. Dehydration may likely occur under non-equilibrium conditions

476   in xenoliths involved in volcanic processes. Nevertheless, the stability, or mestability, of the

477   anhydrous (or partially-hydrous) form of cancrinite is reported in the literature (*e.g.* Ballirano et al.

478   1995; Hassan et al. 2006; Gatta et al. 2014) and is also confirmed by its occurrence in xenoliths

479   within alkaline basalts (Zubkova et al. 2011). The experiments on the *T*-induced dehydration of

480   cancrinite under equilibrium conditions (Sirbescu and Jenkins 1999; Gatta et al. 2014) suggests that

481   this process would occur at temperatures not lower than 650-750 K, at 0.0001 GPa. The combined

482   effect of *P* and *T* on the behavior of cancrinite-group minerals is basically unknown, and this, on

483   one hand, hinders a deep discussion on the petrological implications but, on the other hand, should

484   act as a stimulus for new experiments in this direction. The sub-solidus stabilities of some

485   cancrinite-group minerals were studied by Edgar (1964), who reported that cancrinite and

486   hydroxycancrinite were still stable at 1070 K and 0.13 GPa $P(H_2O)$, suggesting that, at a high-

487   enough carbonate fugacity, cancrinite should be stable at liquidus conditions.

488   The experimental findings of the host-guest interactions and of the structural deformation

489   mechanisms at high *T* and *P* show the relevant role played by the extraframework constituents, and

490   in particular of the cage population (Figure 2), on the behavior of cancrinite-group minerals at non-

491   ambient conditions. The *T*-induced mutual migration of K and Na between channels and cages in

492   pitiglianoite, at temperature above the dehydration process (Bonaccorsi et al. 2007), suggests the

493   potential high-thermal stability of the K-bearing members of the group, which should be further

494   investigated at high-*T* conditions. The modeling of the host-guest interactions at non-ambient

495   conditions provides a more robust background for the potential application of these compounds in

496   several technological fields: for example, by defining the high-*T* stability for a safe use of hydrous

497   cancrinite-subgroup compounds as solid storage-materials of alkaline wastes or for tailoring

498   preparation processes (Bao et al. 2005; Riley et al. 2012). Common precipitation of cancrinite-

499   group compounds were also reported from caustic nuclear waste solutions (*e.g.* Buck and

500   McNamara 2004; Rivera et al. 2011; Wang and Um 2013). The knowledge of the host-guest

501   interactions in cancrinite-group materials with the structural cages occupied by large monovalent

502   cations (*e.g.* K^+, Cs^+, Rb^+) is still poor, as well as their behavior under *T* or *P*. This configuration is

503   shown only by tiptopite (which contains K^+) among the mineralogical species, but the synthesis of

504   several Cs-cancrinites has successfully been reported (*e.g.* Colella and de' Gennaro 1989; Norby et

505   al. 1991; Lee et al. 2000; Fechtelkord et al. 2001; Bieniok et al. 2005; Gatta and Lee 2008), whose

506   thermal (and compressional) stability is still unknown. The confinement of Cs^+ (or Rb^+) cations

507   inside the *can* units, with their small effective pore widths (*sensu* Baerlocher et al. 2007), suggests

508   the potential application of cancrinite-group minerals as nuclear waste storage materials, as recently

509   reported for other classes of microporous materials (*e.g.* Gatta et al. 2008b, 2009a, 2009b, 2012b;

510   Sanchez-Valle et al. 2010). In this light, experiments on the thermo-elastic behavior, (*P,T*)-phase

511   stability and chemical stability (by leaching processes) of Cs-cancrinites are necessary, for their

512   potential utilization.

513   The behavior at non-ambient conditions of the cancrinite-group minerals shows, beside the

514   potential destabilizing effects of temperature (*e.g.* dehydration in the cancrinite subgroup, $P6_3$-to-

515    $P6_3/m$ phase transition in the compounds of davyne subgroup), a high-*P* stability (at room-*T*), which

516   is quite surprising if we consider their microporous nature. The *P*-induced stability is the effect of a

517   structural flexibility, which in turn is based mainly on tilting of rigid tetrahedra around O atoms that

518   behave as hinges. In cancrinite-group minerals, the *P*-induced tilting of tetrahedra usually leads to

519   continuous re-arrangements of the framework without any phase transition. As observed in other

520   classes of open-framework silicates (*e.g.* zeolites), flexibility and microporosity do not necessarily

521   imply high compressibility: the cancrinite-group minerals are less or similarly compressible than

522   other rock-forming minerals (*e.g.* α-quartz, Angel et al. 1997; Na-rich feldspars, Benusa et al. 2005;

523   tri- and di-octahedral micas, Zanazzi and Pavese 2002). In this light, the high-*P* experimental

524 findings on cancrinite-group minerals, here reviewed, corroborate the conclusion of Gatta (2008) on

525 zeolites, which can also be extended to this group of feldspathoids: "*porous does not mean soft*".

526

527

References

Angel, R.J. (2000) Equations of state. In R.M. Hazen, and R.T. Downs, Eds., High-Temperature and High-Pressure Crystal Chemistry, 41, p. 35-60. Reviews in Mineralogy and Geochemistry, Mineralogical Society of America and Geochemical Society, Chantilly, Virginia.

Angel, R.J., Allan, D.R., Miletich, R., and Finger, L.W. (1997) The use of quartz as an internal pressure standard in high-pressure crystallography. Journal of Applied Crystallography, 30, 461-466.

Angel, R.J., Alvaro, M., and Gonzalez-Platas, J. (2014) EosFit7c and a Fortran module (library) for equation of state calculations. Zeitschrift für Kristallographie , 229, 405-419.

Baerlocher, C., McCusker, L.B., and Olson, D.H. (2007) Atlas of Zeolite Framework Types, 6th ed., 398 p. Elsevier, Amsterdam.

Ballirano, P., Maras, A., Caminiti, R., and Sadun, C. (1995) Carbonate-cancrinite: in situ real-time thermal processes studied by means of energy-dispersive X-ray powder-diffractometry. Powder Diffraction , 10, 173-177.

550   Bao, Y., Grutzek, M.W., and Jantzen, C.M. (2005) Preparation and properties of

551   hydroceramic waste forms made with simulated Hanford low-acitivity waste. Journal of American

552   Ceramic Society , 88, 3287-3302.

553   Bell, K., Dunworth, E.A., Bulakh, A.G., and Ivanikov, V.V. (1996) Alkaline rocks of the

554   Turiy pensisula, Russia, including type-locality turjaite and turjite: a review. Canadian Mineralogist

555   , 34, 265-280.

556   Benusa, M.T., Angel, R.J., and Ross, N.L.(2005) Compression of Albite, $NaAlSi_3O_8$.

557   American Mineralogist, 90, 1115-1120.

558   Berman, R.G. (1988) Internally-consistent thermodynamic data for minerals in the system

559   $Na_2O-K_2O-CaO-MgO-FeO-Fe_2O_3-Al_2O_3-SiO_2-TiO_2-H_2O-CO_2$. Journal of Petrology, 29, 445-522.

560   Bieniok, A., Brendel, U., Paulus, E.F., and Amthauer, G. (2005) Microporous cobalto- and

561   zinco-phosphates with the framework-type of cancrinite. European Journal of Mineralogy, 17, 813-

562   818.

563   Birch, F. (1947) Finite elastic strain of cubic crystals. Physical Review, 71, 809-824.

564   Bonaccorsi, E., and Merlino, S. (2005) Modular microporous minerals: cancrinite-davyne

565   group and C-S-H phases. In G. Ferraris, and S. Merlino, Eds., Micro- and Mesoporous Mineral

566   Phases, 57, p. 241-290. Reviewsin Mineralogy and Geochemistry, Mineralogical Society of

567   America and Geochemical Society, Chantilly, Virginia.

568   Bonaccorsi, E., Merlino, S., and Pasero, M. (1990). Davyne: its structural relationship with

569   cancrinite and vishnevite. Neues Jahrbuch für Mineralogie-Monatshefte, 97-112.

570   Bonaccorsi, E., Merlino, S., Orlandi, P., Pasero, M., and Vezzalini, G. (1994) Quadridavyne

571   $[(Na,K)_6Cl_2][Ca_2Cl_2][Si_6Al_6O_{24}]$, a new feldspathoid mineral from Vesuvius area. European Journal

572   of Mineralogy, 6, 481-487.

573   Bonaccorsi, E., Comodi, P., and Merlino, S. (1995) Thermal behaviour of davyne-group

574   minerals. Physics and Chemistry of Minerals, 22, 367-374.

575   Bonaccorsi, E., Merlino, S., Pasero, M., and Macedonio, G. (2001) Microsommite: crystal

576   chemistry, phase transitions, Ising model and Monte Carlo simulations. Physics and Chemistry of

577   Minerals, 28, 509-522.

578   Bonaccorsi, E., Della Ventura, G., Bellatreccia, F., and Merlino, S. (2007) The thermal

579   behaviour and dehydration of pitiglianoite, a mineral of the cancrinite-group. Microporous and

580   Mesoporous Materials, 99, 225-235.

581   Brigatti, M.F., and Guggenheim, S. (2002) Mica crystal chemistry and the influence of

582   pressure, temperature and solid solution on atomistic models. In A. Mottana, F.P. Sassi, J.B.

583   Thompson, and S. Guggenheim, Micas: Crystal Chemistry and Metamorphic Petrology, 46, p. 1-98.

584   Reviews in Mineralogy and Geochemistry, Mineralogical Society of America and Geochemical

585   Society, Chantilly, Virginia.

586   Buck, E.C., and McNamara, B.K. (2004) Precipitation of nitrate-cancrinite in Hanford tank-

587   sludge. Environmental Science and Technology, 38, 4432-4438.

588   Chukanov, N.V., Pekov, I.V., Olysych, L.V., Massa, W., Yakubovich, O.V., Zadov, A.E.,

589   Rastsvetaeva, R.K., and Vigasina, M.F. (2010a) Kyanoxalite, a new cancrinite-group mineral

590   species with extraframework oxalate anion from the Lovozero alkaline pluton, Kola peninsula.

591   Geology of Ore Deposits, 52, 778-790.

592   Chukanov, N.V., Zubkova, N.V., Pekov, I.V., Olysych, L.V., Bonaccorsi, E., and

593   Pushcharovsky, D.Y. (2010b). Balliranoite, $(Na,K)_6Ca_2(Si_6Al_6O_{24})Cl_2(CO_3)$, a new cancrinite-group

594   mineral from Monte Somma - Vesuvio volcanic complex, Italy. European Journal of Mineralogy,

595   22, 113-119.

596   Colella, C., and de' Gennaro, M. (1989) Cancrinite crystallization from alkaline

597   aluminosilicate systems containing large and small cations. In M.L. Occelli, and H.E. Robson,

598   Zeolite synthesis, 398, p. 196-208. ACS Symposium Series, American Chemical Society.

599   Deer, W.A., Howie, R.A., Wise, W.S., and Zussman, J. (2004) Rock-forming minerals.

600   Framework silicates: silica minerals, feldspathoids and the zeolites, Vol. 4B, The Geological

601   Society, London.

602   Della Ventura, G., Bellatreccia, F., and Bonaccorsi, E. (2005) CO_2 in minerals of the

603   cancrinite-sodalite group: pitiglianoite. European Journal of Mineralogy, 17, 847-851.

604   Della Ventura, G., Bellatreccia, F., Parodi, G.C., Càmara, F., and Piccinini, M. (2007)

605   Single-crystal FTIR and X-ray study of vishnevite, ideally $[Na_6(SO_4)][Na_2(H_2O)_2](Si_6Al_6O_{24})$.

606   American Mineralogist , 92, 713-721.

607   Della Ventura, G., Bellatreccia, F., and Piccinini, M. (2008) Channel CO_2 in feldspathoids:

608   new data and new perspectives. Rendiconti Lincei-Scienze Fisiche e Naturali, 19, 141-159.

609   Edgar, A.D. (1964) Studies on cancrinites: II – Stability fields and cell dimensions of

610   potassium and potassium-rich cancrinites. Canadian Mineralogist, 8, 53-67.

611   Edgar, A.D. (1984) Chemistry, occurrence and paragenesis of feldspathoids: A review. In

612   W.L. Brown, Ed., Feldspars and Feldspathoids: Structures, Properties and Occurrences, 137, 501-

613   532. NATO ASI Series, Series C: Mathematical and Physical Sciences.

614   Erd, R.C., and Czamanske, G.K. (1983) Orickite and coyoteite, two new sulfides minerals

615   from Coyote Peak, Humboldt County, California. American Mineralogist, 68, 245-254.

616   Fall, A., Bodnar, R.J., Szabò, C., and Pàl-Molnàr, E. (2007) Fluid evolution in the nepheline

617   syenite of the Ditrau alkaline massif, Tansylvania, Romania. Lithos , 91, 331-345.

618   Fechtelkord, M., Posnatzki, B., Buhl, J.-C., Fyfe, C.A., Groat, L.A., and Raudsepp, M.

619   (2001) Characterization of synthetic Cs-Li cancrinite grown in a butanediol-water system; an NMR

620   spectroscopic and Rietveld refinement study. American Mineralogist, 86, 881-888.

621   Foit, F.F., Peacor, D.R., and Heinrich, E.W. (1973) Cancrinite with a new superstructure

622   from Bancroft, Ontario. Canadian Mineralogist, 11, 940-951.

623   Fulignati, P., Panichi, C., Sbrana, A., Caliro, S., Gioncada, A., and Del Moro, A. (2005)

624   Skarn formation at the walls of the 79 AD magma chamber of Vesuvius (Italy): mineralogical and

625   isotopic constraints. Neues Jahrbuch für Mineralogie-Abhandlungen, 181/1, 53-66.

626   Gatta, G.D. (2008) Does porous mean soft? On the elastic behaviour and structural evolution

627   of zeolites under pressure. Zeitschrift für Kristallographie, 223, 160-170.

628   Gatta G.D. (2010) Extreme deformation mechanisms in open-framework silicates at high-

629   pressure: Evidence of anomalous inter-tetrahedral angles. Microporous and Mesoporous Materials,

630   128, 78–84.

631   Gatta, G.D. and Angel, R.J. (2007) Elastic behavior and pressure-induced structural

632   evolution of nepheline: implications for the nature of the modulated superstructure. American

633   Mineralogist, 92, 1446-1455.

634   Gatta, G.D., and Lee, Y. (2008) Pressure-induced structural evolution and elastic behaviour

635   of $Na_6Cs_2Ga_6Ge_6O_{24} \cdot Ge(OH)_6$ variant of cancrinite: A synchrotron powder diffraction study.

636   Microporous and Mesoporous Materials, 116, 51-58.

637   Gatta, G.D. and Lee, Y. (2014) Zeolites at high pressure: A review. Mineralogical

638   Magazine, 78, 267-291.

639   Gatta, G.D., Nestola, F., and Boffa Ballaran, T. (2006) Elastic behavior, phase transition and

640   pressure induced structural evolution of analcime. American Mineralogist, 91, 568-578.

641   Gatta, G.D., Rotiroti, N., Boffa Ballaran, T., and Pavese, A. (2008a) Leucite at high-

642   pressure: elastic behaviour, phase stability and petrological implications. American Mineralogist,

643   93, 1588-1596.

644   Gatta, G.D., Rotiroti, N., Zanazzi, P.F., Rieder, M., Drabek, M., Weiss, Z., and Klaska, R.

645   (2008b) Synthesis and crystal structure of the feldspathoid $CsAlSiO_4$: an open-framework silicate

646   and potential nuclear waste disposal phase. American Mineralogist, 93, 988-995.

647   Gatta, G.D., Rinaldi, R., McIntyre, G.J., Nénert, G., Bellatreccia, F., Guastoni, A., and Della

648   Ventura, G. (2009a) On the crystal structure and crystal chemistry of pollucite,

649    $(Cs,Na)_{16}Al_{16}Si_{32}O_{96} \cdot nH_2O$: a natural microporous material of interest in nuclear technology.

650   American Mineralogist, 94, 1560-1568.

651   Gatta, G.D., Rotiroti, N., Boffa Ballaran, T., Sanchez-Valle, C., and Pavese, A. (2009b)

652   Elastic behavior and phase-stability of pollucite, a potential host for nuclear waste. American

653   Mineralogist, 94, 1137-1143.

654   Gatta, G.D., Angel, R.J., and Carpenter, M.A. (2010) Low-temperature behaviour of natural

655   kalsilite with $P31c$ symmetry: an in-situ single-crystal X-ray diffraction study. American

656   Mineralogist, 95, 1027-1034.

657   Gatta, G.D., Angel, R.J., Zhao, J., Alvaro, M., Rotiroti, N., and Carpenter, M.A. (2011)

658   Phase stability, elastic behavior, and pressure-induced structural evolution of kalsilite: A ceramic

659   material and high-T/high-P mineral. American Mineralogist, 96, 1363–1372.

660   Gatta, G.D., Lotti, P., Kahlenberg, V., and Haefeker, U. (2012a) The low-temperature

661   behaviour of cancrinite: an in situ single-crystal X-ray diffraction study. Mineralogical Magazine,

662   76, 933-948.

663   Gatta, G.D., Merlini, M., Lotti, P., Lausi, A., and Rieder, M. (2012b) Phase stability and

664   thermo-elastic behavior of CsAlSiO4 (ABW): A potential nuclear waste disposal material.

665   Microporous and Mesoporous Materials, 163, 147–152.

666   Gatta, G.D., Lotti, P., Nénert, G., and Kahlenberg, V. (2013a) On the crystal structure and

667   low-temperature behaviour of davyne: A single-crystal X-ray and neutron diffraction study.

668   Microporous and Mesoporous Materials, 185, 137-148.

669   Gatta, G.D., Lotti, P., and Kahlenberg, V. (2013b) The low-temperature behavior of

670   balliranoite (CAN topology): An in situ single-crystal X-ray diffraction study. Microporous and

671   Mesoporous Materials, 174, 44-53.

672   Gatta, G.D., Comboni, D., Alvaro, M., Lotti, P., Càmara, F., and Domeneghetti, M.C.

673   (2014) Thermoelastic behavior and dehydration process of cancrinite. Physics and Chemestry of

674   Minerals, 41, 373-386.

675   Gies, H., Kirchner, R., van Koningsveld, H., and Treacey, M.M.J. (1999) Faulted Zeolite

676   framework structures. Proc. 12th International Zeolite Conference, Baltimore, Maryland, U.S.A.,

677   July 5-11, 1998; eds. M.M.J. Treacey, B.K. Marcus, M.E. Bisher, J.B. Higgins, Materials Research

678   Society, Warrendale, Pennsylvania, 2999-3029.

679   Grossman, L. (1980) Refractory inclusions in the Allende meteorite. Annual Review of

680   Earth and Planetary Sciences, 8, 559-608.

681   Grundy, H.D., and Hassan, I. (1982) The crystal structure of a carbonate-rich cancrinite.

682   Canadian Mineralogist, 20, 239-251.

683   Harlow, G.E., and Bender, W. (2013) A study of ruby (corundum) composition from the

684   Mogok Belt, Myanmar: searching for chemical fingerprints. American Mineralogist, 98, 1120-1132.

685   Hassan, I. (1996a) The thermal behavior of cancrinite. Canadian Mineralogist, 34, 893-900.

686   Hassan, I. (1996b) Thermal expansion of cancrinite. Mineralogical Magazine, 60, 949-956.

687   Hassan, I., and Grundy, H.D. (1984) The character of cancrinite-vishnevite solid solution

688   series. Canadian Mineralogist, 22, 333-340.

689   Hassan, I., and Grundy, H.D. (1990) Structure of davyne and implications for stacking

690   faults. Canadian Mineralogist, 28, 341-349.

691   Hassan, I., and Buseck, P.R. (1992) The origin of the superstructure and modulations in

692   cancrinite. Canadian Mineralogist, 30, 49-59.

693   Hassan, I., Antao, S.M., and Parise, J.B. (2006) Cancrinite: Crystal structure, phase

694   transitions and dehydration behavior with temperature. American Mineralogist, 91, 1117-1124.

695   Holland, T.J.B. and Powell, R. (2011) An improved and extended internally consistent

696   thermodynamic dataset for phases of petrological interest, involving a new equation of state for

697   solids. Journal of Metamorphic Geology, 29, 333–383.

698   Isupova, D., Ida, A., Kihara, K., Morishita, T., and Bulka, G. (2010) Asymmetric thermal

699   vibrations of atoms and pyroelectricity in cancrinite. Journal of Mineralogical and Petrological

700   Sciences, 105, 29-41.

701   Jarchow, O. (1965) Atomanordnung und strukturverfeinerung von cancrinit. Zeitschrift für

702   Kristallographie, 122, 407-422.

703   Lee, Y., Parise, J.B., Tripathi, A., Kim, S.J., and Vogt, T. (2000) Synthesis and crystal

704   structures of gallium and germanium variants of cancrinite. Microporous and Mesoporous

705   Materials, 39, 445-455.

706   Löns, J. and Schulz, H. (1967) Strukturverfeinerung von Sodalith, $Na_8Si_6Al_6O_{24}Cl_2$. Acta

707   Crystallographica, 23, 434-436.

708   Lotti, P. (2014) Cancrinite-group minerals at non-ambient conditions: a model of the elastic

709   behavior and structure evolution. Ph.D. thesis, University of Milan (Italy), p. 306.

710   Lotti, P., Gatta, G.D., Rotiroti, N., and Càmara, F. (2012) High-pressure study of a natural

711   cancrinite. American Mineralogist, 97, 872-882.

712   Lotti, P., Gatta, G.D., Merlini, M., and Hanfland, M. (2014a) High-pressure behavior of

713   davyne [CAN-topology]: An in situ single-crystal synchrotron diffraction study. Microporous and

714   Mesoporous Materials, 198, 203-214.

715   Lotti, P., Gatta, G.D., Rotiroti, N., Càmara, F., and Harlow, G.E. (2014b) The high-pressure

716   behavior of balliranoite: a cancrinite-group mineral. Zeitschrift für Kristallographie , 229, 63-76.

717   Merlino, S. (1984) Feldspathoids: Their average and real structures. In W.L. Brown, Ed.,

718   Feldspars and Feldspathoids: Structures, Properties and Occurrences, 137, p. 435-470. NATO ASI

719   Series, Series C: Mathematical and Physical Sciences.

720   Merlino, S., Mellini, M., Bonaccorsi, E., Pasero, M., Leoni, L., and Orlandi, P. (1991)

721   Pitiglianoite, a new feldspathoid from southern Tuscany, Italy: chemical composition and crystal

722   structure. American Mineralogist, 76, 2003-2008.

723   Norby, P., Krogh Andersen, I.G., Krogh Andersen, E., Colella, C., and de' Gennaro, M.

724   (1991) Synthesis and structure of lithium cesium and lithium thallium cancrinites. Zeolites, 11, 248-

725   253.

726   Ogorodova, L.P., Mel'chakova, L.V., Vigasina, M.F., Olysych, L.V., and Pekov, I.V. (2009)

727   Cancrinite and cancrisilite in the Khibina-Lovozero alkaline complex: thermochemical and thermal

728   data. Geochemistry International, 47, 260-267.

729   Oh, J.E., Clark, S.M., and Monteiro, P.J.M. (2011) Determination of the bulk modulus of

730   hydroxycancrinite, a possible zeolitic precursor in geopolymers, by high-pressure synchrotron X-

731   ray diffraction. Cement and Concrete Composites, 33, 1014-1019.

732   Olysych, L.V., Vigasina, M.F., Mel'chakova, L.V., Ogorodova, L.P., Pekov, I.V., and

733   Chukanov, N.V. (2011) Thermal evolution and thermochemistry of the cancrinite-group carbonate-

734   oxalate mineral. Geochemistry International, 49, 731-737.

735   Pauling, L. (1930) The structure of some sodium and calcium aluminosilicates. Proceedings

736   of the National Academyof Sciences, 16, 453-459.

737   Peacor, D.R., Rouse, R.C., and Ahn, J.-H. (1987) Crystal structure of tiptopite, a framework

738   berillophosphate isotypic with basic cancrinite. American Mineralogist, 72, 816-820.

739   Pekov, I.V., Olysych, L.V., Chukanov, N.V., Zubkova, N.V., and Pushcharovsky, D.Y.

740   (2011a). Crystal chemistry of cancrinite-group minerals with an AB type framework: a review and

741   new data. I. Chemical and structural variations. Canadian Mineralogist, 49, 1129-1150.

742   Pekov, I.V., Olysych, L.V., Zubkova, N.V., Chukanov, N.V., Van, K.V., and

743   Pushcharovsky, D.Y. (2011b) Depmeierite $Na_8[Al_6Si_6O_{24}](PO_4,CO_3)_{1-x}*3H_2O$ (x<0.5): a new

744   cancrinite-group mineral species from the Lovozero alkaline pluton of the Kola peninsula. Geology

745   of Ore Deposits, 53, 604-613.

746   Rastsvetaeva, R.K., Pekov, I.V., Chukanov, N.V., Rozenberg, K.A., and Olysych, L.V.

747   (2007) Crystal Structures of Low-Symmetry Cancrinite and Cancrisilite Varieties. Crystallography

748   Report, 52, 811-818.

749   Riley, B.J., Crum, J.V., Matyas, J., McCloy, J.S., and Lepry, W.C. (2012) Solution-derived,

750   chloride-containing minerals as a waste form for alkali chlorides. Journal of American Ceramic

751   Society, 95, 3115-3123.

752   Rivera, N.A., Choi, S., Strepka, C., Mueller, K.T., Chorover, J., and O'Day, P.A. (2011)

753   Cesium and strontium incorporation into zeolite-type phases during homogeneous nucleation from

754   caustic solution. American Mineralogist, 96, 1809-1820.

755   Rouquerol, J., Avnir, D., Fairbridge, C.W., Everett, D.H., Haynes J.M., Pernicone, N.,

756   Ramsay, J.D.F., Sing, K.S.W., and Unger K.K. (1994) Recommendations for the characterization of

757   porous solids (Technical Report). Pure and Applied Chemistry, 66, 1739-1758.

758   Sanchez-Valle, V., Chio, C-H., and Gatta, G.D. (2010) Single-crystal elastic properties of

759    $(Cs,Na)AlSi_2O_6 \cdot H_2O$ pollucite: with potential use for long-term storage of Cs radioisotopes. Journal

760   of Applied Physics, 108, 093509 (1-7).

761   Sapozhnikov, A.N. (2010) Crystal chemical features of davyne from Tultui lazurite deposit

762   (Baikal region). Journal of Structural Chemistry, 51, 507-513.

763   Sindern, S., and Kramm, U. (2000) Volume characteristics and element transfer of fenite

764   aureoles: a case-study from the Iivaara alkaline complex, Finland. Lithos, 51, 75-93.

765   Sirbescu, M., and Jenkins, D.M. (1999) Experiments on the stability of cancrinite in the

766   system $Na_2O-CaO-Al_2O_3-SiO_2-CO_2-H_2O$. American Mineralogist, 84, 1850-1860.

767   Smith, J.V. (2000) Tetrahedral frameworks of zeolites, clathrates and related materials.

768   Landolt-Börnstein - Group IV Physical Chemistry, 14A, 251-266.

769   Wang, G., and Um, W. (2013) Facilitated strontium transport by remobilization of

770   strontium-containing secondary precipitates in Hanford site subsurface. Journal of Hazardous

771   Materials, 248-249, 364-370.

772   Zanazzi, P.F., and Pavese, A. (2002) Behavior of Micas at High-Pressure and High-

773   Temperature. In A. Mottana, F.P. Sassi, J.B. Thompson, and S. Guggenheim, Eds., Micas: Crystal

774   Chemistry and Metamorphic Petrology, 46, p. 99-116. Reviews in Mineralogy and Geochemistry,

775   Mineralogical Society of America and Geochemical Society, Chantilly, Virginia.

776   Zubkova, N.V., Chukanov, N.V., Pekov, I.V., and Pushcharovsky, D.Y. (2011) Low-

777   hydrous cancrinite: atomic structure and indicative importance. Doklady Earth Sciences, 439, 998-

778   1001.

779

780

781 **Table 1.** Cancrinite-group minerals.

782

	Chemical formula, Z	Unit-cell constants (a, c; Å)	Space group	Ref.
Cancrinite subgroup:				
cancrinite	$[(Na,Ca)_6(CO_3)_{1.4-1.7}][Na_2(H_2O)_2][Si_6Al_6O_{24}]$, 1	12.615, 5.127	$P6_3$	*a*
vishnevite	$[(Na,K)_6(SO_4)][Na_2(H_2O)_2][Si_6Al_6O_{24}]$, 1	12.685, 5.179	$P6_3$	*a, b*
hydroxycancrinite	$[Na_6(OH)_2][Na_2(H_2O)_2][Si_6Al_6O_{24}]$, 1	12.740, 5.182	$P3$	*a*
cancrisilite	$Na_7Al_5Si_7O_{24}(CO_3) \cdot 3H_2O$, 1	12.575, 5.105	$P6_3mc$	*a*
pitiglianoite	$[(Na_4K_2)(SO_4)][Na_2(H_2O)_2][Si_6Al_6O_{24}]$, 3	22.121, 5.221	$P6_3$	*a*
kyanoxalite	$[Na_5(C_2O_4)_{0.5-1}(H_2O)_{2-3}][NaH_2O]_2[Si_{6-7}Al_{5-6}O_{24}]$, 1	12.74, 5.21	$P6_3$	*c*
depmeierite	$[Na_6(PO_4)_{0.67}H_2O][NaH_2O]_2[Si_6Al_6O_{24}]$, 1	12.73, 5.18	$P6_3$	*c*
Davyne subgroup:				
davyne	$[(Na,K)_6(SO_4,Cl)][Ca_2Cl_2][Si_6Al_6O_{24}]$, 1	12.705, 5.368	$P6_3/m$ or $P6_3$	*a, d*
balliranoite	$[(Na,Ca)_6(CO_3)_{1.4-1.7}][CaCl]_2[Al_6Si_6O_{24}]$, 1	12.695, 5.325	$P6_3$	*a, e*
microsommite	$[Na_4K_2(SO_4)][Ca_2Cl_2][Si_6Al_6O_{24}]$, 3	22.142, 5.345	$P6_3$	*a*
quadridavyne	$[(Na,K)_6Cl_2][Ca_2Cl_2][Si_6Al_6O_{24}]$, 4	25.771, 5.371	$P6_3/m$	*a*
tiptopite	$[(Li_{2.9}Na_{1.7}Ca_{0.7})(OH)_2(H_2O)_{1.3}][K_2][Be_6P_6O_{24}]$; 1	11.655, 4.692	$P6_3$	*f*

Note: Chemical formulae based on 12 tetrahedral cations. References - *a*: Bonaccorsi and Merlino (2005); *b:* Della Ventura et al. (2007); *c*: Pekov et al. (2011a); *d*: Lotti et al. (2014a); *e*: Lotti et al.(2014b); *f*: Peacor et al. (1987).

783

784

785

786

787

788

789

790

791

792

793

794

795

796

Table 2. Thermo-elastic parameters of cancrinite-group minerals.

		P-range (GPa)	β_{V0} (GPa^{-1})	K_{V0} (GPa)	K_V'		T-range (K)	$\alpha_{V(293K)}$ (10^{-5} K^{-1})
Cancrinite	a	0.0001-4.62	0.022(1)	45(2)	6(1)			
	a	5.00-6.63	0.025(1)	40(2)	4			
	b						298-769	4.2(4)
	c						100-293	3.8(7)
	d						303-748	4.88(8)
	d						748-823	3.1(6)
Vishnevite	e	0.20-2.47	0.020(2)	49(4)	5.4(33)			
	e	3.83-7.40	0.033(3)	30(3)	2.6(5)			
Balliranoite	f	0.0001-6.77	0.021(1)	48(3)	4.0(10)			
	g						108-293	4.6(4)
Davyne ($P6_3$)	h	0.38-7.18	0.0215(5)	46.5(11)	3.7(3)			
	i						110-293	4.2(4)
	j						293-449	5.4(6)[*]
Davyne ($P6_3/m$)	j						503-948	3.0(1)[*]
	j						293-829	2.7(2)[*]
Microsommite ($P6_3$)	j						293-423	5.5(4)[*]
Microsommite ($P6_3/m$)	j						503-947	1.9(2)[*]
Hydroxycancrinite[#]	k	0.0001-6.1	0.0213(4)	46.9(9)	4.0(4)			
Na$_6$Cs$_2$[Ga$_6$Ge$_6$O$_{24}$]·Ge(OH)$_6$[#]	l	0.0001-5.01	0.029(2)	35(2)	11(1)			

		P-range (GPa)	β_{a0} (GPa^{-1})	K_{a0} (GPa)	K_a'		T-range (K)	$\alpha_{a(293K)}$ (10^{-5} K^{-1})
Cancrinite	a	0.0001-4.62	0.0064(7)	52(6)	11(4)			
	a	5.00-6.63	0.0057(4)	58(4)	4			
	b						298-769	0.90(8)
	c						100-293	0.7(2)
	d						303-748	1.16(3)
	d						748-823	0.6(3)
Vishnevite	e	0.20-2.47	0.0060(4)	56(4)	7.3(32)			
	e	3.83-7.40	0.0083(6)	40(3)	1.8(4)			
Balliranoite	f	0.0001-6.77	0.0062(5)	54(4)	4.6(14)			
	g						108-293	1.4(2)
Davyne ($P6_3$)	h	0.38-7.18	0.0066(1)	50.3(9)	4.0(3)			
	i						110-293	1.4(1)
	j						293-449	1.69(8)[*]
Davyne ($P6_3/m$)	j						503-948	1.32(6)[*]
	j						293-829	1.34(7)
Microsommite ($P6_3$)	j						293-423	1.6(1)[*]
Microsommite ($P6_3/m$)	j						503-947	0.86(4)[*]
Hydroxycancrinite[#]	k	0.0001-6.1	0.0062(6)[*]	54(5)[*]	4[*]			
Na$_6$Cs$_2$[Ga$_6$Ge$_6$O$_{24}$]·Ge(OH)$_6$[#]	l	0.0001-5.01	0.0083(4)	40(2)	11(1)			

		P-range (GPa)	β_{c0} (GPa^{-1})	K_{c0} (GPa)	K_c'	K_{a0}/K_{c0}	T-range (K)	$\alpha_{c(293K)}$ (10^{-5} K^{-1})	α_{c0}/α_{a0}
Cancrinite	a	0.0001-4.62	0.0098(6)	34(2)	2.8(8)	1.53			
	a	5.00-6.63	0.016(1)	20.6(14)	4	2.82			
	b						298-769	2.3(2)	2.55
	c						100-293	2.1(3)	3.00
	d						303-748	2.58(8)	2.22
	d						748-823	1.9(5)	3.17
Vishnevite	e	0.20-2.47	0.0090(5)	37(2)	5.0(20)	1.51			
	e	3.83-7.40	0.021(4)	16(3)	3.6(5)	2.50			
Balliranoite	f	0.0001-6.77	0.0083(4)	40(2)	3.3(6)	1.35			
	g						108-293	1.7(2)	1.21
Davyne ($P6_3$)	h	0.38-7.18	0.0083(1)	40.3(7)	3.2(2)	1.25			
	i						110-293	1.6(1)	1.14
	j						293-449	1.6(4)	0.95
Davyne ($P6_3/m$)	j						503-948	0.3(1)	0.23
	j						293-829	0.11(3)[*]	0.08
Microsommite ($P6_3$)	j						293-423	1.6(4)	1.00
Microsommite ($P6_3/m$)	j						503-947	0.2(1)	0.23
Hydroxycancrinite[#]	k	0.0001-6.1	0.0101(9)[*]	33(3)[*]	4[*]	1.64			
Na$_6$Cs$_2$[Ga$_6$Ge$_6$O$_{24}$]·Ge(OH)$_6$[#]	l	0.0001-5.01	0.0108(3)	31(1)	7.4(8)	1.29			

Note: β_{V0} is the isothermal compressibility coefficient, K_{V0} and K_V' are the isothermal bulk modulus and its P-derivative, respectively, and $\alpha_{V(293K)}$ is the thermal expansion coefficient of the unit-cell volume; β_{j0}, K_{j0}, K_j', and $\alpha_{j(293K)}$ are the co-respective axial coefficients (with $j = a$, c);

References - *a*: Lotti et al. (2012); *b*: Hassan et al. (2006); *c*: Gatta et al. (2012a); *d*: Gatta et al. (2014); *e*: Lotti (2014); *f*: Lotti et al. (2014b); *g*: Gatta et al. (2013b); *h*: Lotti et al. (2014a); *i*: Gatta et al. (2013a); *j*: Bonaccorsi et al. (1995); *k*: Oh et al. (2010); *l*: Gatta and Lee (2008); * Calculated from published data; # Synthetic compounds.

Table 3 (deposited). Relevant inter-tetrahedral angles (°), voids diameters (Å), bond distances (Å) and the ditrigonal rotation angle (°) at different pressures of cancrinite-group minerals.

P (GPa)	Si-O1-Al	Si-O2-Al	Si-O3-Al	Si-O4-Al	O3-O4-O3	$\alpha_{S6R\perp[0001]}$	O3-O4$_{S4R}$	O1-O1$_{12R}$	O3-O4$_{12R}$	(Na,Ca)-O1	(Na,Ca)-O2
						Cancrinite (Lotti et al. 2012)					
0.0001	147.5(7)	151.8(6)	131.4(6)	132.5(5)	142.9(4)	8.8(2)	4.15(1)	9.16(1)	8.48(1)	2.888(8)	2.441(7)
0.76(2)	145.4(7)	149.0(5)	131.3(6)	132.6(5)	141.1(4)	9.6(2)	4.08(1)	9.12(1)	8.51(2)	2.883(8)	2.397(6)
0.99(2)	145.9(7)	149.5(5)	132.2(5)	131.5(5)	143.1(3)	9.5(2)	4.13(1)	9.08(1)	8.41(1)	2.879(8)	2.403(6)
1.39(2)	143.9(6)	148.3(5)	131.3(4)	129.9(5)	140.3(3)	10.0(2)	4.09(1)	9.04(1)	8.432(9)	2.886(7)	2.380(6)
2.33(2)	143.6(6)	148.5(4)	130.4(4)	129.4(4)	140.1(3)	9.8(2)	4.07(1)	9.00(1)	8.388(8)	2.867(7)	2.374(6)
3.59(2)	141.4(7)	144.2(5)	128.9(5)	128.6(5)	136.5(3)	11.6(2)	3.99(1)	8.88(1)	8.405(8)	2.894(7)	2.312(6)
4.30(3)	140.7(6)	143.3(5)	128.6(5)	127.8(5)	135.7(3)	12.2(2)	3.97(1)	8.81(1)	8.380(8)	2.902(7)	2.286(7)
5.00(2)	139.6(6)	143.6(5)	127.7(4)	127.2(4)	135.1(3)	11.6(2)	3.98(1)	8.837(9)	8.351(8)	2.874(7)	2.291(6)
5.73(3)	137.6(7)	140.9(5)	126.0(5)	126.5(5)	133.1(4)	13.2(2)	3.91(1)	8.68(1)	8.377(9)	2.931(8)	2.262(7)
6.16(2)	138.3(6)	140.7(5)	126.8(5)	126.9(5)	132.8(3)	13.2(2)	3.89(1)	8.70(1)	8.386(8)	2.914(7)	2.252(6)
6.63(3)	137.3(6)	138.6(5)	126.4(5)	126.8(5)	133.0(3)	14.3(2)	3.87(1)	8.636(9)	8.379(8)	2.932(7)	2.219(6)
						Vishnevite (Lotti 2014)					
0.0001	153.0(7)	147.6(6)	139.9(6)	141.2(6)	152.5(4)	10.2(2)	4.025(12)	8.943(7)	8.750(8)	2.942(6)[Na1] 2.901(4)[Na2]	2.465(7)[Na1] 2.365(5)[Na2]
0.52(2)	151.9(9)	149.1(6)	138.3(9)	137.2(8)	147.5(5)	9.0(2)	4.01(2)	8.978(13)	8.725(17)	2.897(10)[Na1] 2.859(9)[Na2]	2.485(10)[Na1] 2.388(7)[Na2]
1.20(3)	150.2(8)	148.6(6)	137.4(9)	136.0(9)	146.2(5)	9.3(2)	3.99(3)	8.913(14)	8.695(18)	2.898(10)[Na1] 2.865(9)[Na2]	2.463(11)[Na1] 2.375(7)[Na2]
1.78(5)	149.0(9)	146.8(7)	135.8(8)	136.0(9)	145.1(5)	10.0(3)	3.98(2)	8.874(15)	8.670(18)	2.899(10)[Na1] 2.866(10)[Na2]	2.432(11)[Na1] 2.341(8)[Na2]
2.47(2)	147.8(10)	146.3(7)	135.5(9)	136.2(8)	144.8(5)	10.3(3)	3.96(2)	8.816(15)	8.642(18)	2.892(12)[Na1] 2.868(10)[Na2]	2.402(17)[Na1] 2.327(10)[Na2]
3.24(9)	147.4(9)	144.3(7)	132.6(8)	132.6(8)	141.5(5)	10.8(3)	3.98(2)	8.768(14)	8.558(16)	2.903(11)[Na1] 2.858(9)[Na2]	2.408(15)[Na1] 2.304(9)[Na2]

3.43(4)	145.0(8)	145.9(7)	134.4(8)	133.5(7)	141.5(5)	10.5(2)	3.93(2)	8.737(15)	8.594(17)	2.889(10)^{Na1} 2.861(9)^{Na2}	2.401(13)^{Na1} 2.316(9)^{Na2}
4.23(7)	143.1(8)	144.5(7)	131.5(7)	130.0(7)	137.7(4)	11.4(3)	3.92(2)	8.596(13)	8.513(15)	2.905(9)^{Na1} 2.881(9)^{Na2}	2.367(11)^{Na1} 2.274(9)^{Na2}
5.74(6)	142.5(9)	143.4(7)	128.9(7)	130.7(7)	136.0(4)	12.4(3)	3.90(2)	8.506(15)	8.493(17)	2.943(10)^{Na1} 2.901(10)^{Na2}	2.371(12)^{Na1} 2.244(9)^{Na2}
6.10(8)	143.3(9)	142.6(7)	128.0(8)	129.5(8)	135.0(5)	12.7(3)	3.87(3)	8.449(15)	8.473(18)	2.956(11)^{Na1} 2.900(9)^{Na2}	2.367(13)^{Na1} 2.229(9)^{Na2}
6.11(4)	138.9(9)	140.0(7)	128.4(8)	128.3(8)	135.3(5)	14.4(3)	3.84(3)	8.260(16)	8.43(2)	2.984(11)^{Na1} 2.956(10)^{Na2}	2.290(14)^{Na1} 2.173(9)^{Na2}
7.40(4)	136.2(10)	130.0(7)	125.1(13)	125.2(14)	129.9(10)	17.5(4)	3.71(3)	8.18(2)	8.916(16)	2.942(12)^{Na1} 2.96(2)^{Na2}	2.078(17)^{Na1} 2.008(15)^{Na2}

Balliranoite (Lotti et al. 2014b)

0.0001	155.4(3)	160.3(3)	136.1(4)	137.9(4)	161.4(2)	1.2(1)	4.400(10)	9.400(7)	8.279(11)	2.614(4)	2.560(4)
0.85(3)	152.9(3)	160.2(3)	133.7(4)	136.4(5)	157.7(2)	1.4(1)	4.399(10)	9.323(8)	8.202(11)	2.610(5)	2.551(4)
1.73(3)	150.3(3)	159.4(3)	132.5(4)	134.7(4)	154.4(2)	1.8(1)	4.392(10)	9.255(8)	8.173(10)	2.623(4)	2.544(4)
2.62(4)	148.4(3)	159.4(3)	131.7(4)	133.3(4)	152.8(2)	1.9(1)	4.390(10)	9.189(8)	8.120(11)	2.624(4)	2.542(4)
3.80(5)	146.4(3)	158.5(3)	130.5(4)	131.6(4)	148.8(2)	2.4(1)	4.357(10)	9.087(8)	8.077(9)	2.631(5)	2.525(4)
4.95(3)	144.6(3)	159.3(3)	129.0(4)	130.2(4)	146.9(2)	2.3(2)	4.354(11)	9.008(8)	8.015(11)	2.632(5)	2.536(4)
4.95(4)	143.6(3)	157.9(4)	128.6(5)	128.5(5)	145.3(3)	2.7(2)	4.333(12)	8.940(10)	7.964(13)	2.626(7)	2.513(5)
6.77(2)	142.3(3)	156.7(3)	127.5(4)	128.1(4)	143.8(2)	2.9(2)	4.339(10)	8.927(8)	7.947(11)	2.625(6)	2.504(5)

Davyne (Lotti et al. 2014a)

0.0001[*]	167.7(3)	158.1(3)	142.0(2)	-	180	2.5(1)	4.361(6)	9.451(6)	8.439(4)	2.661(4)	2.533(4)
0.38(2)	169.1(6)	157.1(4)	139.9(5)	142.6(5)	170.1(4)	3.0(2)	4.328(11)	9.414(11)	8.460(11)	2.676(7)^{Ca1} 2.681(7)^{Ca2}	2.521(6)^{Ca1} 2.522(6)^{Ca2}
0.91(3)	164.2(6)	157.6(4)	140.1(5)	139.9(5)	168.6(3)	2.9(2)	4.344(8)	9.377(10)	8.403(8)	2.680(7)^{Ca1} 2.672(7)^{Ca2}	2.517(5)^{Ca1} 2.532(6)^{Ca2}
1.57(5)	159.3(6)	156.2(4)	139.0(4)	138.2(4)	162.6(3)	3.6(2)	4.325(8)	9.301(9)	8.373(8)	2.683(7)^{Ca1} 2.680(7)^{Ca2}	2.490(5)^{Ca1} 2.510(6)^{Ca2}
2.05(6)	157.5(5)	156.7(4)	137.3(4)	137.7(4)	160.8(2)	3.4(2)	4.328(7)	9.280(9)	8.329(7)	2.700(7)^{Ca1} 2.668(7)^{Ca2}	2.487(5)^{Ca1} 2.513(6)^{Ca2}

3.07(2)	154.6(5)	155.2(4)	134.5(3)	137.2(4)	157.3(2)	4.0(2)	4.327(11)	9.192(9)	8.264(7)	2.674(7)[Ca1] 2.674(7)[Ca2]	2.462(5)[Ca1] 2.491(6)[Ca2]
3.49(2)	153.4(5)	156.0(4)	134.4(3)	137.0(3)	156.2(2)	3.5(2)	4.304(11)	9.187(8)	8.254(7)	2.655(5)[Ca1] 2.656(7)[Ca2]	2.473(5)[Ca1] 2.495(6)[Ca2]
4.56(7)	151.1(6)	155.7(5)	132.9(4)	136.0(4)	153.2(2)	3.6(2)	4.287(14)	9.129(9)	8.207(8)	2.649(7)[Ca1] 2.650(7)[Ca2]	2.460(6)[Ca1] 2.490(7)[Ca2]
5.33(8)	149.9(6)	156.2(5)	131.7(4)	134.4(4)	152.0(3)	3.6(2)	4.293(14)	9.064(9)	8.160(8)	2.656(6)[Ca1] 2.658(7)[Ca2]	2.470(6)[Ca1] 2.505(7)[Ca2]
6.10(8)	148.8(7)	155.6(5)	129.9(4)	133.8(4)	150.2(3)	3.9(2)	4.290(15)	9.011(9)	8.113(9)	2.655(6)[Ca1] 2.659(6)[Ca2]	2.455(6)[Ca1] 2.494(7)[Ca2]
7.18(6)	148.0(7)	155.1(6)	129.2(5)	133.3(5)	147.9(3)	4.1(2)	4.254(16)	8.953(11)	8.090(10)	2.647(8)[Ca1] 2.655(8)[Ca2]	2.443(8)[Ca1] 2.483(9)[Ca2]

$\alpha_{S6R\perp[0001]}$ = $\Sigma_i\{1/6\cdot[|120°-\theta_i|/2]\}$ (see Figure 6; parameter originally defined for phyllosilicates, Brigatti and Guggenheim 2002)
* $P6_3/m$ davyne sample at 0.0001 GPa, $P6_3$ davyne at all the other pressures (Lotti et al. 2014a).

801

802 **Table 4 (deposited).** Relevant inter-tetrahedral angles (°), voids diameters (Å), bond distances (Å) and the ditrigonal rotation angle (°) at different
803 temperatures of cancrinite-group minerals.

T (K)	Si-O1-Al	Si-O2-Al	Si-O3-Al	Si-O4-Al	O3-O4-O3	$\alpha_{S6R\perp[0001]}$	O3-O4$_{S4R}$	O1-O1$_{12R}$	O3-O4$_{12R}$	(Na,Ca)-O1	(Na,Ca)-O2
					Cancrinite (Hassan et al. 2006)						
298	151.6(6)	155.3(5)	142.7(10)	125.2(9)	146.8*	7.63*	4.160*	8.793*	8.447*	2.888(7)	2.521(6)
374	152.2(6)	155.5(5)	142.8(10)	126.1(9)	147.8*	7.18*	4.157*	8.814*	8.457*	2.881(7)	2.524(6)
480	152.7(6)	155.8(5)	142.3(11)	127.2(11)	148.8*	7.08*	4.167*	8.845*	8.461*	2.871(7)	2.531(6)
571	152.8(6)	156.3(5)	140.5(12)	129.9(13)	150.9*	6.70*	4.186*	8.884*	8.456*	2.861(6)	2.543(6)
678	152.9(6)	156.7(4)	138.4(14)	135.3(16)	154.0*	6.40*	4.189*	8.931*	8.465*	2.850(7)	2.567(5)
769	153.7(6)	157.8(4)	139.2(11)	134.1(11)	154.7*	5.98*	4.189*	8.953*	8.486*	2.852(7)	2.587(5)
784	153.4(6)	157.6(4)	139.0(10)	134.0(11)	154.6*	5.95*	4.186*	8.959*	8.487*	2.847(7)	2.586(5)
830	152.2(6)	158.3(4)	140.3(9)	132.5(9)	154.3*	6.05*	4.206*	8.941*	8.478*	2.857(7)	2.596(5)
875	151.0(6)	157.8(4)	140.1(10)	132.9(10)	154.3*	5.90*	4.202*	8.989*	8.490*	2.838(7)	2.593(5)
921	151.8(6)	158.4(4)	140.1(9)	132.4(10)	155.3*	5.90*	4.229*	8.971*	8.474*	2.851(7)	2.599(5)
966	152.4(6)	158.9(4)	139.6(9)	132.7(10)	155.7*	5.78*	4.242*	8.973*	8.468*	2.852(7)	2.603(5)
1073	155.1(7)	158.7(5)	138.6(9)	133.2(10)	157.7*	5.75*	4.256*	8.972*	8.470*	2.866(7)	2.604(6)
1164	156.1(7)	159.5(5)	139.8(11)	133.5(11)	159.9*	5.60*	4.285*	8.976*	8.461*	2.876(8)	2.622(6)
1225	154.5(10)	160.6(6)	141.0(16)	134.7(15)	162.9*	4.78*	4.270*	9.052*	8.499*	2.837(9)	2.639(8)
					Cancrinite (Isupova et al. 2010)						
173	146.4(1)	151.1(1)	133.2(2)	133.18(8)	144.9*	9.03*	4.134*	8.800*	8.475*	2.877(2)	2.429(2)
293	147.4(1)	151.86(9)	133.8(2)	133.71(7)	145.7*	8.43*	4.144*	8.856*	8.493*	2.866(2)	2.444(2)
473	149.8(2)	153.2(2)	135.1(2)	135.0(2)	149.2*	7.73*	4.163*	8.923*	8.502*	2.854(2)	2.469(3)
673	151.5(2)	152.2(2)	136.6(2)	136.2(2)	151.5*	7.95*	4.146*	8.950*	8.540*	2.857(3)	2.461(4)
					Cancrinite (Gatta et al. 2014)						
303	147.2(2)	151.2(2)	133.4(2)	133.3(2)	144.6(3)	8.48(9)	4.145(6)	8.862(5)	8.487(4)	2.862(3)	2.437(4)
478	148.0(2)	152.5(2)	134.0(2)	134.1(2)	146.39(16)	7.99(8)	4.166(6)	8.901(5)	8.485(4)	2.854(2)	2.455(3)

748	151.2(3)	151.0(3)	136.1(3)	136.6(3)	149.8(2)	8.19(12)	4.155(8)	8.971(7)	8.536(5)	2.846(3)	2.446(4)

Cancrinite (Gatta et al. 2012a)

293	147.02(9)	151.79(7)	133.46(7)	133.55(7)	144.84(2)	8.45(3)	4.129(3)	8.841(2)	8.486(1)	2.858(1)	2.437(1)
250	146.46(8)	151.45(10)	133.26(7)	133.26(7)	144.42(5)	8.66(3)	4.123(2)	8.815(2)	8.471(1)	2.863(1)	2.429(1)
220	146.14(8)	151.27(10)	133.05(6)	133.02(6)	143.98(4)	8.75(3)	4.120(2)	8.810(2)	8.475(1)	2.866(1)	2.427(1)
180	145.85(8)	150.90(9)	132.83(7)	132.85(7)	143.71(5)	8.87(3)	4.117(2)	8.802(2)	8.472(1)	2.866(1)	2.421(1)
140	145.42(8)	150.74(9)	132.78(7)	132.72(7)	143.37(5)	9.05(3)	4.111(2)	8.783(2)	8.474(1)	2.873(1)	2.418(1)
100	145.32(7)	150.56(9)	132.55(7)	132.66(7)	143.05(5)	9.09(3)	4.108(2)	8.783(1)	8.480(1)	2.875(1)	2.416(1)

Vishnevite (Lotti 2014)

293	153.3(2)	147.4(3)	140.6(4)	140.2(4)	152.6(2)	10.2(1)	4.042(10)	8.930(5)	8.726(7)	2.920(3)	2.411(4)
110	151.6(2)	146.8(2)	139.6(4)	139.4(4)	151.2(2)	10.8(1)	4.015(10)	8.852(5)	8.715(6)	2.937(3)	2.400(4)

Balliranoite (Gatta et al. 2013b)

293	155.98(8)	161.28(6)	136.44(6)	137.33(7)	162.68(5)	1.02(3)	4.427(1)	9.387(1)	8.251(2)	2.6218(9)	2.5761(8)
250	155.27(8)	161.28(7)	136.13(6)	137.09(6)	161.81(4)	1.03(3)	4.424(1)	9.373(2)	8.239(2)	2.620(1)	2.5752(9)
220	154.81(7)	161.21(6)	135.98(6)	136.84(6)	161.43(4)	1.04(3)	4.430(1)	9.372(2)	8.235(2)	2.6207(9)	2.5753(8)
180	154.32(8)	161.17(6)	135.70(6)	136.65(6)	160.85(4)	1.07(3)	4.428(1)	9.367(2)	8.231(2)	2.6209(9)	2.5746(9)
140	153.92(8)	161.23(7)	135.51(6)	136.42(6)	160.43(4)	1.06(6)	4.427(1)	9.356(2)	8.219(2)	2.619(1)	2.5738(9)
108	153.65(8)	161.21(7)	135.40(6)	136.29(7)	160.18(4)	1.08(3)	4.429(1)	9.352(6)	8.215(2)	2.620(1)	2.5741(9)

Davyne (Gatta et al. 2013a)

293	166.15(7)	156.87(5)	141.83(7)	141.52(6)	171.51(4)	3.00(2)	4.331(2)	9.427(1)	8.467(1)	2.6715(8)	2.5162(7)
250	164.87(6)	156.96(5)	141.85(6)	141.24(5)	169.96(4)	3.00(2)	4.323(2)	9.413(1)	8.460(1)	2.6701(7)	2.5153(7)
220	164.02(5)	156.80(4)	141.43(5)	141.06(4)	169.00(3)	3.00(2)	4.327(1)	9.412(1)	8.4512(8)	2.6675(6)	2.5129(6)
180	163.05(5)	156.88(4)	141.24(5)	140.73(4)	167.92(3)	3.00(2)	4.327(1)	9.404(1)	8.4459(8)	2.6685(6)	2.5140(6)
140	162.45(5)	156.77(4)	141.05(5)	140.29(4)	167.22(3)	3.02(2)	4.331(1)	9.400(1)	8.4357(8)	2.6670(6)	2.5121(6)
110	161.99(5)	156.73(4)	140.86(5)	140.26(4)	166.65(3)	3.04(2)	4.329(1)	9.394(1)	8.4334(8)	2.6677(6)	2.5117(6)

Pitiglianoite** (Bonaccorsi et al. 2007)

298	155.9(4)	144.9(4)	143.2(4)	144.0(4)	155.7*	11.25*	4.000*	8.953*	8.835*	2.954(5)^{Na}	2.394(6)^{Na}
730	152.7(5)	147.9(6)	139.3(6)	139.6(7)	152.0*	10.03*	4.051*	8.942*	8.730*	2.917(9)^{Na}	2.42(1)^{Na} 2.82(1)^{K}
298 post-HT	147.9(3)	148.0(2)	136.8(2)	136.5(2)	147.6*	10.00*	4.078*	8.868*	8.646*	2.911(4)^{Na} 3.122(4)^{K}	2.397(8)^{Na} 2.760(5)^{K}

$\alpha_{S6R\perp[0001]} = \Sigma_i\{1/6\cdot[|120°-\theta_i|/2]\}$ (see Figure 6; parameter originally defined for phyllosilicates, Brigatti and Guggenheim 2002)
*Calculated from published data; ** Structure refinements performed in the vishnevite subcell.

804

44

805 **Figures Captions**

806 **Figure 1**. *(Top left)* The hexagonal array of single six-membered rings of tetrahedra in the plane
807 perpendicular to the **c**-axis (S6R⊥[0001]). (*Top right*) A portion of a column of *can* units. Two
808 base-sharing cages are shown, along with a portion of a *dzc* chain. *(Bottom left)* The [CAN]
809 framework viewed down [0001] of davyne and *(bottom right)* cancrinite. The S6R⊥[0001] cage-
810 bases, the large 12R-channel and the S4R-units are shown.

811 **Figure 2.** (*Top*) Schematic view of the Na-H_2O and Ca-Cl chains in the columns of *can* units of
812 cancrinite- and davyne-subgroup minerals, respectively. (*Bottom*) Cage-Na^+ (*left side*) and cage-
813 Ca^{2+} (*right side*) coordination environments in cancrinite and davyne, respectively. Dashed lines
814 represent mutually exclusive bonds.

815 **Figure 3.** (*Left side*) Schematic view (down the **c**-axis) of the extraframework population in the
816 channels of cancrinite-group minerals, showing the cationic sites (C), close to the channel walls,
817 and the anions/molecules positions, at the center of the channel. (*Middle*) Coordination shell of the
818 (Na^+,Ca^{2+}) cations in the channels of cancrinite and balliranoite. (*Right side*) The two possible and
819 mutually exclusive configurations of the channel population in vishnevite and davyne: the SO_4^{2-}
820 group can coexist with an "external" Na site at the same *z* coordinate, but it is mutually exclusive
821 with the "internal" K site. If the maximum content of one SO_4^{2-} per formula unit is reached, the
822 channel must be internally ordered. The potential upward and downward configurations of the SO_4^{2-}
823 tetrahedra are shown. Dashed lines represent mutually exclusive bonds.

824 **Figure 4.** The pressure-induced evolution of the unit cell volume, and *a* and *c* cell edges of
825 cancrinite (Lotti et al. 2012), vishnevite (Lotti 2014), balliranoite (Lotti et al. 2014b) and davyne
826 (Lotti et al. 2014a).

827 **Figure 5.** The inter-tetrahedral O3-O4-O3 angle in $P6_3$ davyne (*left side*) is symmetry-induced to
828 O3-O3-O3 = 180° in $P6_3/m$ davyne (*right side*), for the presence of mirror planes at *z* = 0.25 and
829 0.75.

830 **Figure 6.** The [CAN] framework of cancrinite viewed down [0001] (*left side*) and two base-sharing
831 *can* units (*right side*) showing the relevant structural parameters (diameters and angles) reported in
832 Tables 3 and 4.

833 **Figure 7.** The pressure-induced evolution of the inter-tetrahedral Si-O1-Al (squares), Si-O2-Al
834 (circles), Si-O3-Al (triangles) and Si-O4-Al (diamonds) angles of cancrinite (Lotti et al. 2012),
835 vishnevite (Lotti 2014), balliranoite (Lotti et al. 2014b) and davyne (Lotti et al. 2014a).

836

837

838

839

840

841 **Figure 1**. *(Top left)* The hexagonal array of single six-membered rings of tetrahedra in the plane
842 perpendicular to the **c**-axis (S6R⊥[0001]). *(Top right)* A portion of a column of *can* units. Two
843 base-sharing cages are shown, along with a portion of a *dzc* chain. *(Bottom left)* The [CAN]
844 framework viewed down [0001] of davyne and *(bottom right)* cancrinite. The S6R⊥[0001] cage-
845 bases, the large 12R-channel and the S4R-units are shown.
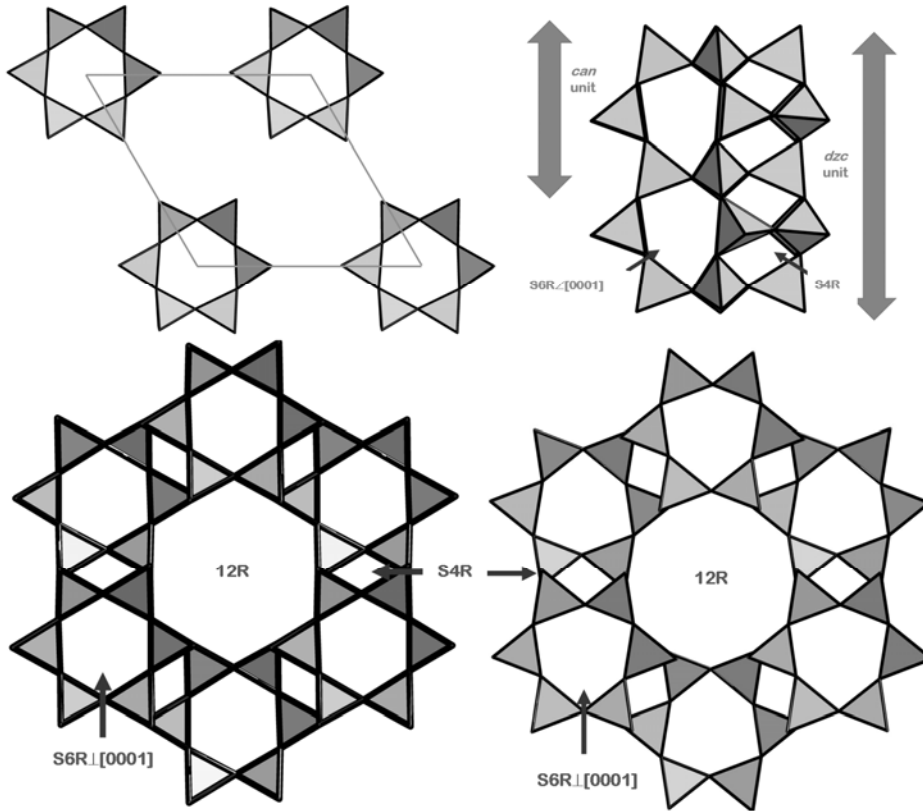
846

847

848 **Figure 2.** (*Top*) Schematic view of the Na-H$_2$O and Ca-Cl chains in the columns of *can* units of
849 cancrinite- and davyne-subgroup minerals, respectively. (*Bottom*) Cage-Na$^+$ (*left side*) and cage-
850 Ca^{2+} (*right side*) coordination environments in cancrinite and davyne, respectively. Dashed lines
851 represent mutually exclusive bonds.
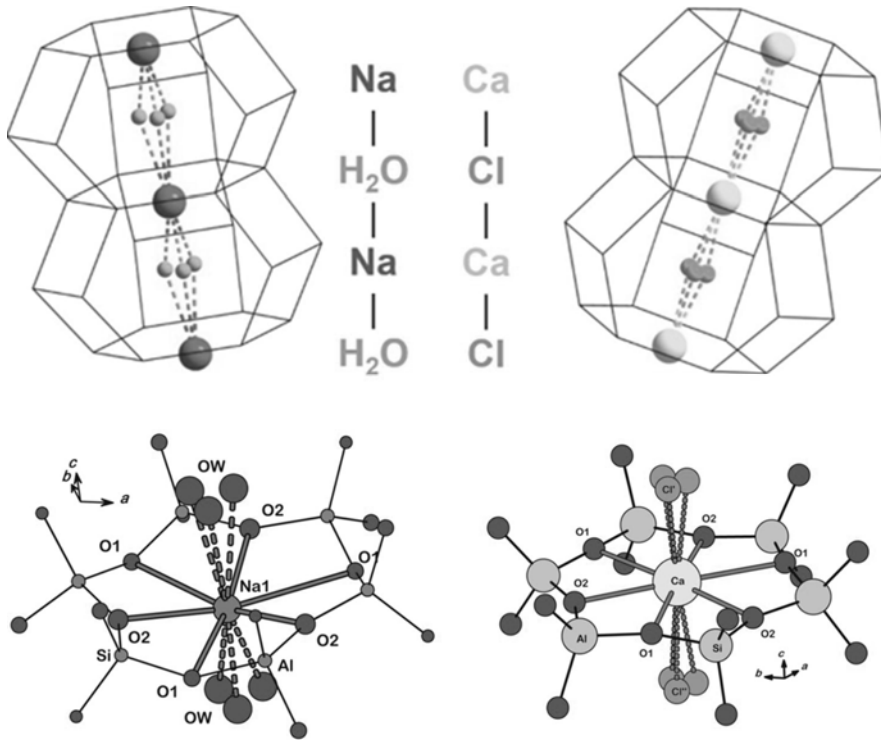
852

853

854 **Figure 3.** (*Left side*) Schematic view (down the **c**-axis) of the extraframework population in the
855 channels of cancrinite-group minerals, showing the cationic sites (C), close to the channel walls,
856 and the anions/molecules positions, at the center of the channel. (*Middle*) Coordination shell of the
857 (Na^+,Ca^{2+}) cations in the channels of cancrinite and balliranoite. (*Right side*) The two possible and
858 mutually exclusive configurations of the channel population in vishnevite and davyne: the SO_4^{2-}
859 group can coexist with an "external" Na site at the same *z* coordinate, but it is mutually exclusive
860 with the "internal" K site. If the maximum content of one SO_4^{2-} per formula unit is reached, the
861 channel must be internally ordered. The potential upward and downward configurations of the SO_4^{2-}
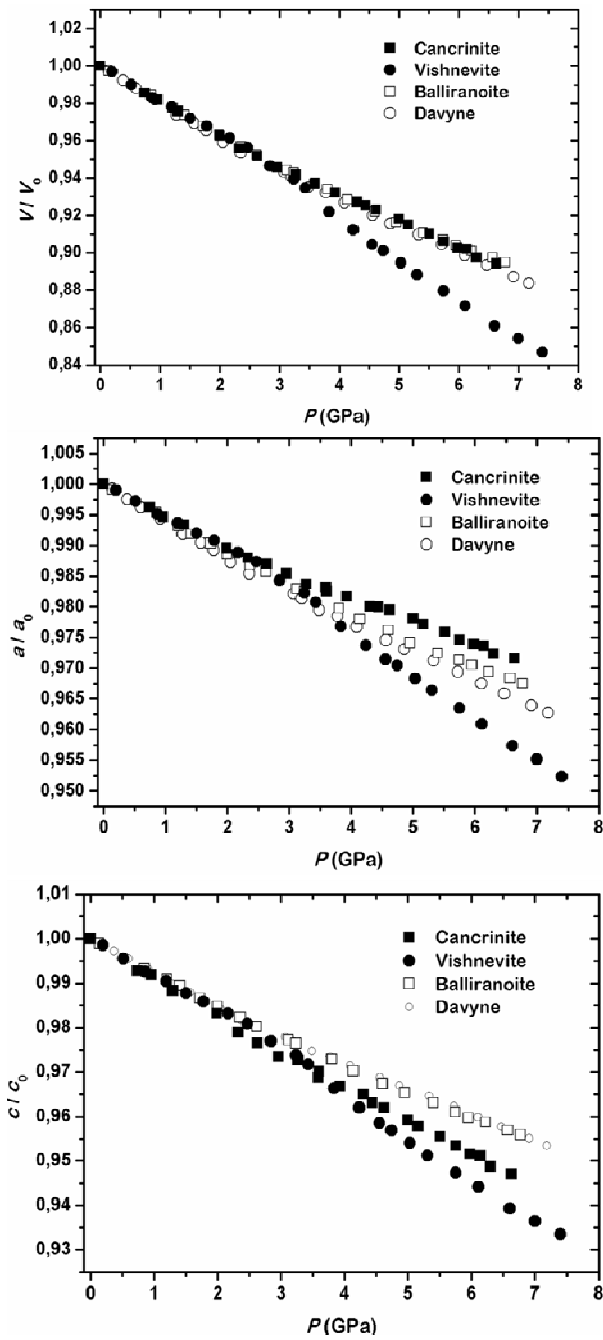862 tetrahedra are shown. Dashed lines represent mutually exclusive bonds.

863
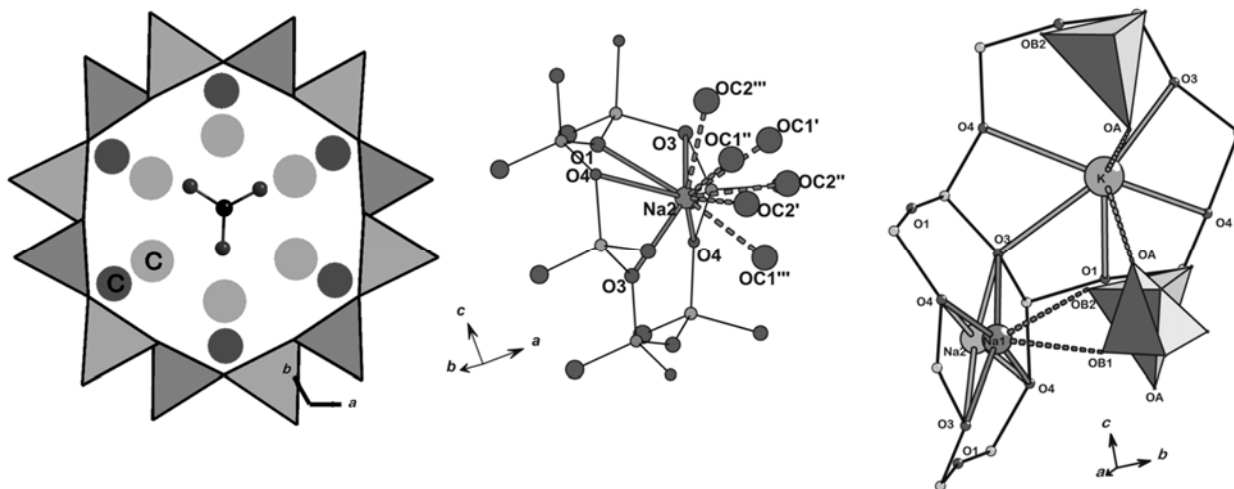
864

865

866 **Figure 4.** The pressure-induced evolution of the unit cell volume, and *a* and *c* cell edges of
867 cancrinite (Lotti et al. 2012), vishnevite (Lotti 2014), balliranoite (Lotti et al. 2014b) and davyne
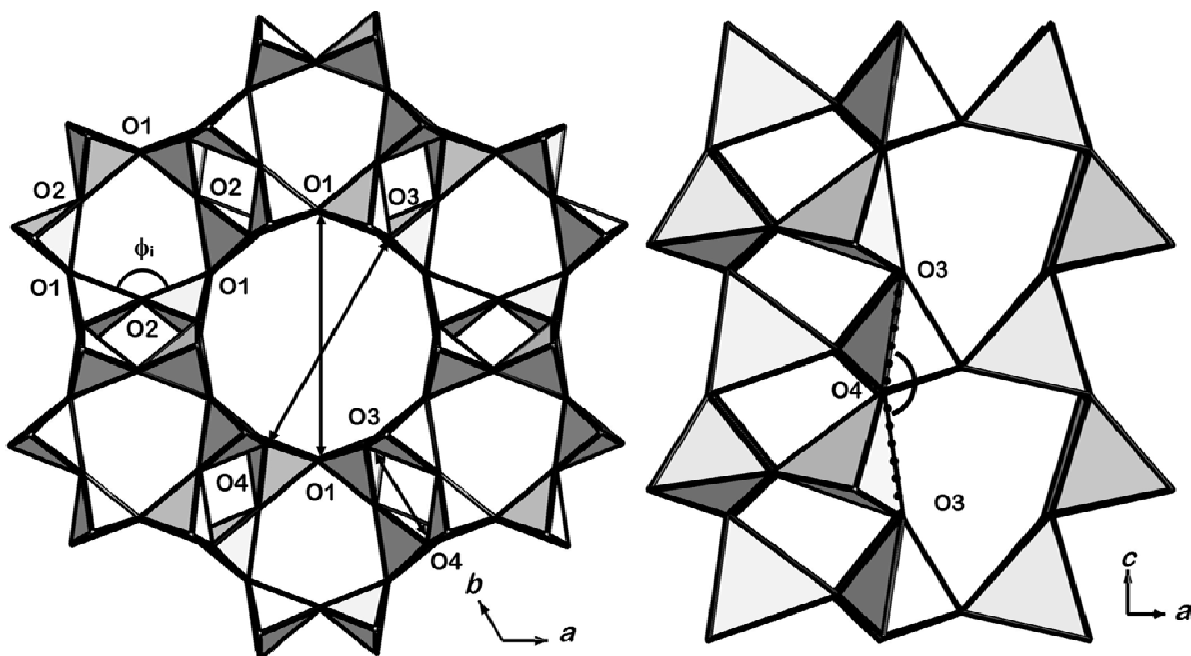868 (Lotti et al. 2014a).

871   **Figure 5.** The inter-tetrahedral O3-O4-O3 angle in $P6_3$ davyne (*left side*) is symmetry-induced to
872   O3-O3-O3 = 180° in $P6_3/m$ davyne (*right side*), for the presence of mirror planes at z = 0.25 and
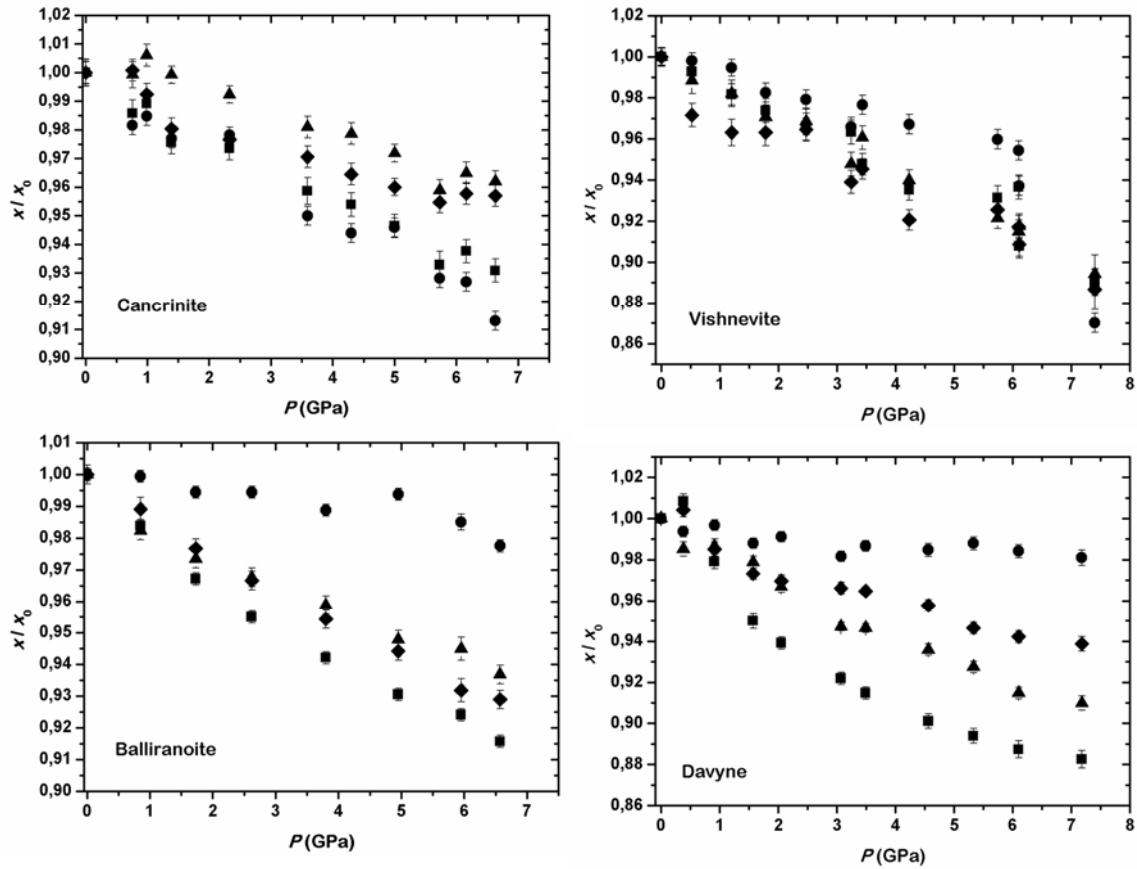873   0.75.
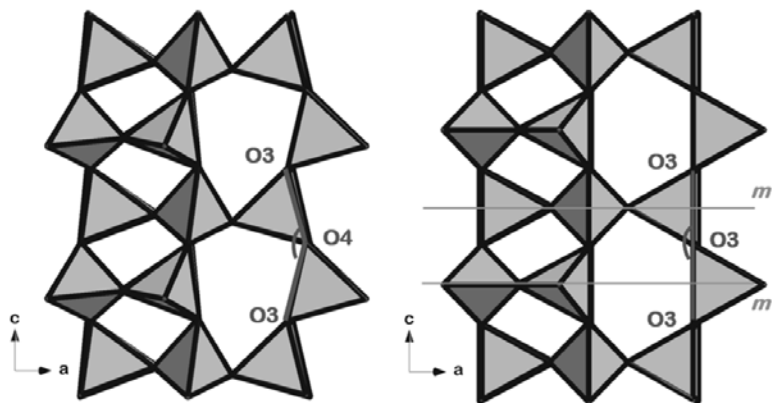
874

875

876 **Figure 6.** The [CAN] framework of cancrinite viewed down [0001] (*left side*) and two base-sharing
877 *can* units (*right side*) showing the relevant structural parameters (diameters and angles) reported in
878 Tables 3 and 4 (deposited).

879

880

881 **Figure 7.** The pressure-induced evolution of the inter-tetrahedral Si-O1-Al (squares), Si-O2-Al
882 (circles), Si-O3-Al (triangles) and Si-O4-Al (diamonds) angles of cancrinite (Lotti et al. 2012),
883 vishnevite (Lotti 2014), balliranoite (Lotti et al. 2014b) and davyne (Lotti et al. 2014a).

884

can unit

dzc unit

S6R∠[0001]

S4R

12R

S4R

S6R⊥[0001]

12R

S6R⊥[0001]

Na — H₂O — Na — H₂O   Ca — Cl — Ca — Cl